

Impact of Static Disorder and Dephasing on Quantum Transport in LH1-RC Models.

Stephon Alexander¹, Roger Andrews², Oliver Fox³, and Sarben Sarkar⁴

¹*Brown Theoretical Physics Center and Department of Physics,
Brown University, Providence, Rhode Island 02912, USA*

²*Department of Physics, The University of the West Indies, St. Augustine, Trinidad and Tobago*

³*Department of Physics and Astronomy, University of Exeter, Exeter EX4 4QL, United Kingdom and*

⁴*Department of Physics, King's College London, Strand, London WC2R 2LS, United Kingdom*

(Dated: September 24, 2025)

We numerically study excitation transfer in an artificial LH1-RC complex—an N -site donor ring coupled to a central acceptor—driven by a narrowband optical mode and evolved under a Lindblad master equation with loss and dephasing. In the absence of disorder, the light-driven system exhibits a tall, narrow on-resonance efficiency peak (near unity for our parameters); dephasing lowers and narrows this peak without shifting its position. Off resonance, the efficiency shows environmentally assisted transport with a clear non-monotonic dependence on dephasing and a finite optimum. Under static disorder, two regimes emerge: photon-ring coupling and diagonal energetic disorder mixes the drive into dark ring modes, activates dissipative channels, and depresses efficiency over a detuning window, whereas intra-ring coupling disorder has a much smaller impact in the tested range; increasing the intra-ring coupling g moves dark-mode crossings away from the operating detuning and restores near-peak performance. In the ordered, symmetric, single-excitation, narrowband limit we *analytically derive* closed-form transfer efficiencies by projecting onto the $k=0$ bright mode and solving the photon-bright mode-acceptor trimer via a Laplace/linear-algebra (determinant) formula; these expressions include a probability-conservation identity $\eta + \sum_k L_k = 1$ that benchmarks the simulations and quantitatively predicts the resonant line shape and its dephasing-induced narrowing. A minimal ring toy model further reproduces coherent trapping and its relief by moderate dephasing (ENAQT). These analytics are exact in the ordered limit and serve as mechanistic guides outside this limit, yielding practical design rules for robust, bio-inspired light harvesting devices.

I. INTRODUCTION

The study of quantum excitation transfer in biological systems and effects such as quantum coherence, disorder and environmental interactions on excitation transfer has demonstrated their biological advantage in harnessing light in light-harvesting (LH) systems [1–3]. LH complexes consist of chromophores, which are protein pigments that capture and transfer photons from sunlight to a reaction center (RC) that initiates the photosynthetic process in organisms [4–6].

Coherent energy transfer in structured quantum networks is a central theme in the study of open quantum systems, with implications for quantum transport, decoherence, and control. One striking physical realization of such dynamics is found in photosynthetic light-harvesting systems, where networks of coupled chromophores transfer excitations with high efficiency despite environmental noise and static disorder. These observations have inspired the development of *artificial analogs*—engineered quantum networks that allow precise tuning of coherence, coupling, and dissipation.

In this work, we analyze excitation transfer in an *artificial ring-central acceptor model*—a driven quantum network inspired by the LH1-RC architecture of purple bacteria. The system consists of a ring of N two-level donor sites coherently coupled to each other and to a central two-level acceptor. An incident photon injects an excitation into the system, which then evolves under a *Lindblad master equation* incorporating loss, dephasing,

and static disorder. This geometry supports a natural decomposition into bright and dark modes, enabling exact reductions and analytic access to key transport features.

Our study is motivated by several threads in the quantum transport literature:

- a) The *Haken-Strobl model* demonstrated how environmental noise induces a transition from coherent to diffusive transport by disrupting phase coherence [7]. The fluctuating forces described in the Haken-Strobl model represents dephasing in the system, which has been shown to be an important effect in light-harvesting photosynthetic systems [8–10].
- b) Models of *environmentally assisted quantum transport* (ENAQT) have shown that moderate dephasing can relieve destructive interference and enhance excitation transfer [11–13].
- c) Conversely, *static disorder* is often associated with Anderson localization [14], though structured disorder can under certain conditions promote delocalization or broaden resonance windows [15–19].

Rebentrost *et al.* [11] investigated how dephasing could be utilized through environmental-assisted quantum transport (ENAQT). They found that optimal transport can be obtained in an Fenna-Matthews-Olson (FMO) light-harvesting system at room temperature by varying the energy detunings and hopping parameters. Plenio and Huelgar [12] considered a dissipative quantum network and found that on-site dephasing can enhance excitation transfer, an effect that was also found in some

classical systems. Chin *et al.* [13] considered an FMO light-harvesting system and found efficiencies above 90% with dephasing-assisted transport. It was found that noise suppressed ineffective pathways thus allowing for increased transfer through more direct channels to the RC. Li *et al.* [8] investigated a chromophore dimer consisting of a donor and acceptor and found that strong noise could allow ENAQT while shutting off vibrationally assisted energy transfer. Xiong *et al.* [10] considered the effects of dissipation and dephasing on source-network-drain models, and by simulating wave-packet dynamics found increased dephasing changed motion from superdiffusive to diffusive. Applying this model to an FMO complex, they found dephasing slightly increased the energy-transfer efficiency.

The effect of disorder on quantum chains is associated with Anderson localization [14], which generally suppresses quantum transport. The general effect of disorder on quantum transport has been studied in many other systems [15–19]. Novo *et al.* [15] investigated quantum transport in a disordered Frenkel-exciton Hamiltonian, and found that in the weak dephasing regime, increasing disorder can on average increase transport efficiency to an optimal value. Žnidarič and Horvat [16] studied the conductivity of an XX spin chain with disorder and dephasing, and determined the optimal dephasing strength and how it scales with differing disorder strengths. Mohseni *et al.* [17] explored geometrical effects in disordered open quantum systems with applications to artificial light-harvesting structures. They found a saturation of the maximum transfer efficiencies for 7 or 14 chromophores, coinciding with the number in the FMO complex and LH2 monomers. Zerah-Harush and Dubi [18] studied the effect of disorder and dephasing on ENAQT with a tight-binding Hamiltonian, and found that disorder can assist in quantum transport even when the system has undergone localization due to the disorder. Maier *et al.* [19] experimentally studied ENAQT on a 10-qubit network with static disorder and variable dephasing noise. They found that increasing noise moved the system away from Anderson localization allowing for improved quantum transport.

The LH1 complex found in purple bacteria is a ring-shaped protein complex surrounding a RC [20–22]. High transfer efficiencies have been found in LH1-RC models under various conditions without disorder and dephasing [23–26]. Other LH1-RC models have investigated the effects of dephasing and disorder [27–31]. Tan and Kuang [27] investigated the effect of ENAQT on LH1 and LH2 systems. Specifically, in the LH2 system, dephasing enhanced the transfer efficiency when the donor-acceptor detuning is below a phase transition critical point. Chuang and Brumer [28] investigated the LH1-RC system including dephasing to model realistic light-matter conditions. They found that transfer rates scaled linearly with the light intensity. Wyke *et al.* [29] investigated the transfer efficiency in an LH1-RC system with a Gaussian pulse and with disorder in the donor-ring en-

ergy separations, and found significantly higher transfer efficiencies. Trinkunas and Freiberg [30] analyzed polarized fluorescence excitation spectra of the disordered LH1 and LH2 complexes. They found that the main disorder in LH1 is structural, whereas in LH2 it is energetic. Van Grondelle and Novoderezhkin [31] determined pathways and time scales for excitation relaxation and measured transient absorption dynamics for the LH1 and LH2 complexes. By doing numerical fits to the transient absorption dynamics, they were able to determine the disordered model parameters.

The main contributions of this paper are as follows:

1. An explicit Lindblad model for a light-driven ring-center system with both structured coherent couplings and site-resolved dissipation and dephasing;
2. An exact reduction in the ordered, symmetric limit to a three-level system (photon-bright mode-acceptor), yielding closed-form expressions for transfer efficiency as a function of detuning and dephasing;
3. A demonstration of how disorder in photon-ring couplings and site energies activates lossy dark modes, degrades performance, and shifts resonance;
4. Identification of regimes where dephasing or increased intra-ring coupling mitigates these effects via mode-mixing or spectral separation.

These results clarify how symmetry and coherence shape transport in open quantum networks, and how noise and disorder can either assist or hinder transfer, depending on the system’s spectral structure. The analytic tractability of the model also provides benchmarks for numerical simulation and design guidance for quantum devices with engineered transport properties.

From an experimental standpoint, the core features of this model—driven collective excitation, tunable dissipation, and network geometry—are increasingly accessible in platforms such as *superconducting qubit arrays*, *trapped ion crystals*, and *photonic lattices* with engineered loss. The bright/dark mode separation, in particular, has direct analogs in cavity-QED and waveguide QED systems where selective coupling plays a central role. Our results may thus inform both the design of synthetic energy transfer devices and the control of excitation flow in programmable quantum simulators.

While our focus is on an artificial system amenable to precise modeling and control, the architecture and mechanisms we study are inspired by natural photosynthetic complexes such as LH1-RC systems in purple bacteria. These biological networks have evolved to exploit coherence and symmetry in noisy environments—a balance that our model captures and extends into regimes relevant for quantum engineering and quantum thermodynamics. In this sense, our work lies at the interface between synthetic quantum systems and biologically motivated quantum transport.

This paper is organized as follows: in Sec. II we introduce the Lindblad open quantum system formalism. We do this for both the ordered system, where a Fourier transform on the donor-ring can be treated as collective modes, and for the disordered system where each donor-ring atom is unique. Analytic results for transfer efficiencies are given for the ordered system. In Sec. III we present our results for the transfer efficiency variation with detuning and dephasing both with and without disorder. We provide an explanation of the high transfer efficiencies in terms of a dark-state mechanism. A conclusion is given in Sec. IV.

II. THEORY

The LH1 antenna system is made up of N 2-LSs coupled with their nearest-neighbors to create a ring structure (see Fig. 1(a)). The Hamiltonian of the ring system, H_d is given as

$$H_d = \sum_{j=1}^N \left[\omega_{d,j} e_j^\dagger e_j + g(e_j^\dagger e_{j+1} + H.c.) \right], \quad (1)$$

where H.c. is Hermitian conjugate, and the annihilation and creation operators, e_j and e_j^\dagger , respectively, are defined as

$$e_j = |0_j\rangle\langle 1_j| \quad e_j^\dagger = |1_j\rangle\langle 0_j|, \quad (2)$$

for $j \in \{1, N\}$, that act on the j^{th} 2-LS donor atom. The j^{th} 2-LS has states $|0_j\rangle$ and $|1_j\rangle$ with corresponding energies 0 and $\omega_{d,j}$. The coupling constant between the j^{th} and $(j+1)^{\text{th}}$ 2-LS is g .

The acceptor site is a 2-LS with Hamiltonian H_a given as

$$H_a = \omega_a a^\dagger a, \quad (3)$$

where a^\dagger (a) is the 2-LS acceptor atom creation (annihilation) operator, and defined as $|1_a\rangle\langle 0_a|$ ($|0_a\rangle\langle 1_a|$). The acceptor has transition frequency ω_a . The interaction Hamiltonian describing the coupling between the acceptor and the ring, H_{da} , is given as

$$H_{da} = \xi \sum_{j=1}^N (e_j^\dagger a + e_j a^\dagger), \quad (4)$$

where ξ is the donor-acceptor coupling constant

The incident photon has Hamiltonian, H_p ,

$$H_p = \omega_p c_p^\dagger c_p, \quad (5)$$

where the photon frequency is ω_p and p defines the mode. The photon annihilation (creation) operator, c_p (c_p^\dagger), are defined as $|1_p\rangle\langle 0_p|$ ($|0_p\rangle\langle 1_p|$). $|0_p\rangle$ and $|1_p\rangle$ are the vacuum and one photon states, respectively. The photon-ring interaction Hamiltonian is given as

$$H_{pd} = \sum_{j=1}^N J_j (c_p^\dagger e_j + c_p e_j^\dagger), \quad (6)$$

where the photon is coupled to each 2-LS on the ring, with j^{th} site-dependent coupling constant J_j .

The full system Hamiltonian, H , is given as

$$\begin{aligned} H &= H_d + H_a + H_p + H_{pd} + H_{da} \\ &= \sum_{j=1}^N \left(\omega_{d,j} e_j^\dagger e_j + g(e_j^\dagger e_{j+1} + H.c.) \right) + \omega_a a^\dagger a \\ &\quad + \omega_p c_p^\dagger c_p + \sum_{j=1}^N \left(J_j (c_p^\dagger e_j + c_p e_j^\dagger) + \xi (e_j^\dagger a + e_j a^\dagger) \right). \end{aligned} \quad (7)$$

A. Lindblad Master Equation

For an arbitrary system with Hamiltonian H' coupled to the environment, the Lindblad master equation which describes the time evolution of the density matrix ρ' is as follows [32, 33]

$$\dot{\rho}' = -i[H', \rho'] + \sum_{n=1}^{N'} \gamma_n \left[L_n \rho' L_n^\dagger - \frac{1}{2} \{L_n^\dagger L_n, \rho'\} \right], \quad (8)$$

where we have a set of N' jump operators, L_n , (along with their Hermitian conjugate L_n^\dagger) and with coupling constants γ_n . The anti-commutator brackets are defined for any pair of operators A and B as $\{A, B\} = AB + BA$. The first term describes the unitary evolution, while the second term describes the incoherent evolution due to coupling with the environment.

For the LH1-RC system, we consider a Lindblad master equation for the density matrix, ρ , of the form

$$\dot{\rho} = -i[H, \rho] + \mathcal{L}_D(\rho) + \mathcal{L}_A(\rho) + \mathcal{L}_P(\rho), \quad (9)$$

where H is any system Hamiltonian, \mathcal{L}_D describes the dissipation via spontaneous emission from the donors to the environment, \mathcal{L}_A describes the charge separation from the acceptor to the reaction center, and \mathcal{L}_P is a dephasing term of the ring due to its coupling to the environment. These superoperators are defined as follows:

$$\mathcal{L}_D(\rho) = \sum_{j=1}^N \kappa (2e_j \rho e_j^\dagger - \{e_j^\dagger e_j, \rho\}), \quad (10a)$$

$$\mathcal{L}_A(\rho) = \Gamma (2a \rho a^\dagger - \{a^\dagger a, \rho\}), \quad (10b)$$

$$\mathcal{L}_P(\rho) = \sum_{j=1}^N \gamma (2e_j^\dagger e_j \rho e_j^\dagger e_j - \{e_j^\dagger e_j, \rho\}), \quad (10c)$$

where 2κ is the spontaneous decay rate of the population of each donor atom on the ring, 2Γ is the spontaneous decay rate of the population of the acceptor to the RC, and 2γ is the dephasing rate of each donor atom.

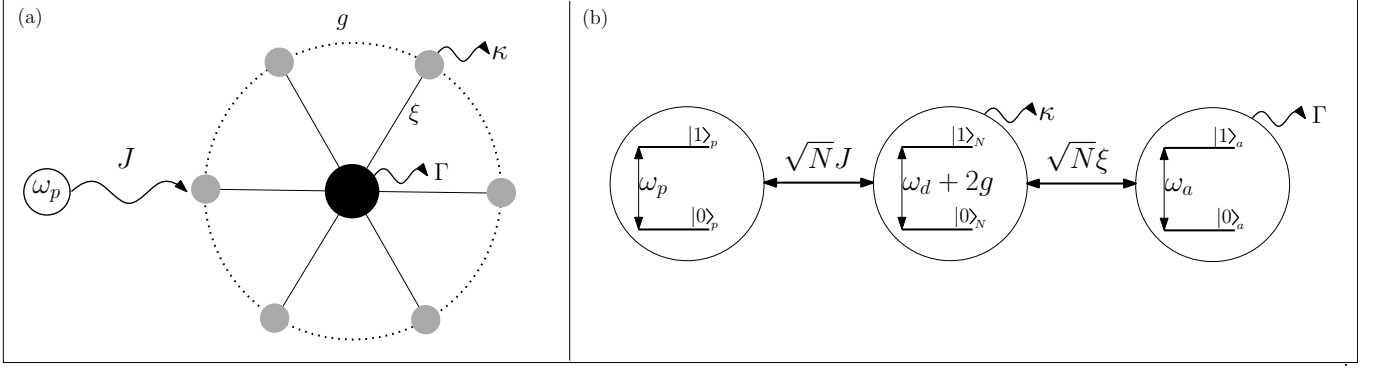


FIG. 1. Schematic showing the ordered LH1-RC system with an incident photon. (a) The N donor-ring atoms (gray), with intra-ring coupling g , and loss rate κ are each coupled to a photon with frequency ω_p and with coupling constant J . Each donor-ring atom is coupled to a central acceptor (black) with coupling constant ξ , and loss rate Γ . (b) A trimer model of the ordered collective LH1-RC ring with an incident photon. The photon is coupled to the collective ring with coupling constant $\sqrt{N}J$, and the collective ring is coupled to the acceptor with coupling constant $\sqrt{N}\xi$. Each 2-LS has energy separation ω_p , $\omega_d + 2g$, and ω_a , for the photon, collective ring, and acceptor, respectively.

B. Collective Description of the LH1 Ring

To solve Eq. (9), we start by considering the case where each donor on the ring is equivalent, which occurs when $\omega_{d,j} = \omega_d$ and $J_j = J$ for every $j \in [1, N]$. We define transition operators e_j and e_j^\dagger in terms of k -space collective operators $\tilde{\mathbf{e}}_k$ and $\tilde{\mathbf{e}}_k^\dagger$ as follows:

$$e_j = \frac{1}{\sqrt{N}} \sum_k e^{i2\pi jk/N} \tilde{\mathbf{e}}_k, \quad (11a)$$

$$e_j^\dagger = \frac{1}{\sqrt{N}} \sum_k e^{-i2\pi jk/N} \tilde{\mathbf{e}}_k^\dagger, \quad (11b)$$

where $k = 0, \dots, N-1$. Substituting Eq. (11a) and (11b) into Eq. (1) (as well as the implied definition of e_{j+1}), we obtain the collective ring Hamiltonian, \tilde{H}_d , as

$$\tilde{H}_d = \sum_{k=0}^{N-1} \omega_k \tilde{\mathbf{e}}_k^\dagger \tilde{\mathbf{e}}_k, \quad (12)$$

where $\omega_k = \omega_d + 2g \cos(k)$ is the energy for each ring mode k . It should be noted that only the $k = 0$ mode couples to the acceptor and the photon, and $\omega_0 = \omega_d + 2g$ is the $k = 0$ mode collective donor-ring energy. The other modes, $k = 1, \dots, N-1$, are decoupled from the photon and the acceptor. Substituting Eq. (11a) and (11b) in Eq. (4) and Eq. (6), gives the collective donor-acceptor and photon-donor Hamiltonians, \tilde{H}_{da} and \tilde{H}_{pd} respectively as

$$\tilde{H}_{da} = \sqrt{N}\xi(\tilde{\mathbf{e}}_0^\dagger a + \tilde{\mathbf{e}}_0 a^\dagger), \quad (13a)$$

$$\tilde{H}_{pd} = \sqrt{N}J(\tilde{\mathbf{e}}_0^\dagger c_p + \tilde{\mathbf{e}}_0 c_p^\dagger). \quad (13b)$$

The Hamiltonian H in Eq. (7) can be rewritten using Eqs. (12), (13a) and (13b), as the collective Hamiltonian \tilde{H} :

$$\begin{aligned} \tilde{H} = & \sum_{k=0}^{N-1} \omega_k \tilde{\mathbf{e}}_k^\dagger \tilde{\mathbf{e}}_k + \omega_a a^\dagger a + \omega_p c_p^\dagger c_p \\ & + \sqrt{N}\xi(\tilde{\mathbf{e}}_0^\dagger a + H.c.) + \sqrt{N}J(c_p^\dagger \tilde{\mathbf{e}}_0 + H.c.). \end{aligned} \quad (14)$$

\tilde{H} can be written into a coupled Hamiltonian, \tilde{H}_c , and a decoupled Hamiltonian, \tilde{H}_D , as $\tilde{H} = \tilde{H}_c + \tilde{H}_D$, where \tilde{H}_c and \tilde{H}_D are defined as

$$\begin{aligned} \tilde{H}_c = & \omega_0 \tilde{\mathbf{e}}_0^\dagger \tilde{\mathbf{e}}_0 + \omega_a a^\dagger a + \omega_p c_p^\dagger c_p \\ & + \sqrt{N}\xi(\tilde{\mathbf{e}}_0^\dagger a + H.c.) + \sqrt{N}J(c_p^\dagger \tilde{\mathbf{e}}_0 + H.c.), \end{aligned} \quad (15a)$$

$$\tilde{H}_D = \sum_{k=1}^{N-1} \omega_k \tilde{\mathbf{e}}_k^\dagger \tilde{\mathbf{e}}_k. \quad (15b)$$

The coupled Hamiltonian, \tilde{H}_c , describes the system shown in the schematic in Fig. 1(b), and can be written in matrix form as

$$\tilde{H}_c = \begin{pmatrix} \omega_p & \sqrt{N}J & 0 \\ \sqrt{N}J & \omega_0 & \sqrt{N}\xi \\ 0 & \sqrt{N}\xi & \omega_a \end{pmatrix}, \quad (16)$$

which acts on the basis states: $\{|1_p, 0_N, 0_a\rangle, |0_p, 1_N, 0_a\rangle, |0_p, 0_N, 1_a\rangle\}$, in the single-excitation subspace. $|1_p, 0_N, 0_a\rangle$ is the single photon state, $|0_p, 1_N, 0_a\rangle$ is the single-excitation donor-ring collective state, and $|0_p, 0_N, 1_a\rangle$ is the single-excitation acceptor state. We denote the eigenvalues of \tilde{H}_c as ϵ_i ($i = 1, 2, 3$), and the eigenvalues of \tilde{H}_D are $\omega_k = \omega_d + 2g \cos(2\pi k/N)$ ($k = 1, \dots, N-1$).

For any operator expectation $\langle O \rangle$, its time derivative satisfies

$$\frac{d\langle O(t) \rangle}{dt} = \text{Tr}[O\dot{\rho}], \quad (17)$$

where Tr represents the trace operation and $\dot{\rho}$ is defined in Eq. (9) for the Hamiltonian \tilde{H} in Eq. (14). Using Eq. (17), we obtain the following coupled equations of motion (derived in Appendix C and D) for the following operator expectation values: $\langle a^\dagger a \rangle$, $\langle c_p^\dagger c_p \rangle$, $\langle \tilde{e}_0^\dagger \tilde{e}_0 \rangle$, $\langle \tilde{e}_k^\dagger \tilde{e}_k \rangle_L$, $\langle \tilde{e}_0^\dagger a \rangle$, $\langle \tilde{e}_0^\dagger c_p \rangle$, and $\langle a^\dagger c_p \rangle$,

$$\frac{d\langle a^\dagger a \rangle}{dt} = -\Gamma \langle a^\dagger a \rangle + i\sqrt{N}\xi(\langle \tilde{e}_0^\dagger a \rangle - \langle a^\dagger \tilde{e}_0 \rangle), \quad (18a)$$

$$\frac{d\langle c_p^\dagger c_p \rangle}{dt} = i\sqrt{N}J(\langle \tilde{e}_0^\dagger c_p \rangle - \langle c_p^\dagger \tilde{e}_0 \rangle), \quad (18b)$$

$$\begin{aligned} \frac{d\langle \tilde{e}_0^\dagger \tilde{e}_0 \rangle}{dt} &= -\left(\kappa + \gamma\left(1 - \frac{1}{N}\right)\right) \langle \tilde{e}_0^\dagger \tilde{e}_0 \rangle + \frac{\gamma}{N} \langle \tilde{e}_k^\dagger \tilde{e}_k \rangle_L \\ &+ i\sqrt{N}\xi(\langle a^\dagger \tilde{e}_0 \rangle - \langle \tilde{e}_0^\dagger a \rangle) + i\sqrt{N}J(\langle c_p^\dagger \tilde{e}_0 \rangle - \langle \tilde{e}_0^\dagger c_p \rangle), \end{aligned} \quad (18c)$$

$$\frac{d\langle \tilde{e}_k^\dagger \tilde{e}_k \rangle_L}{dt} = \left(-\kappa - \frac{\gamma}{N}\right) \langle \tilde{e}_k^\dagger \tilde{e}_k \rangle_L + \gamma\left(1 - \frac{1}{N}\right) \langle \tilde{e}_0^\dagger \tilde{e}_0 \rangle, \quad (18d)$$

$$\begin{aligned} \frac{d\langle \tilde{e}_0^\dagger a \rangle}{dt} &= \left(-i(\Delta - 2g) - \frac{1}{2}(\gamma + \Gamma + \kappa)\right) \langle \tilde{e}_0^\dagger a \rangle \\ &+ i\sqrt{N}\xi(\langle a^\dagger a \rangle - \langle \tilde{e}_0^\dagger \tilde{e}_0 \rangle) + i\sqrt{N}J\langle c_p^\dagger a \rangle, \end{aligned} \quad (18e)$$

$$\begin{aligned} \frac{d\langle \tilde{e}_0^\dagger c_p \rangle}{dt} &= \left(-i(\delta - 2g) - \frac{1}{2}(\gamma + \kappa)\right) \langle \tilde{e}_0^\dagger c_p \rangle \\ &+ i\sqrt{N}J\langle c_p^\dagger c_p \rangle - \langle \tilde{e}_0^\dagger \tilde{e}_0 \rangle + i\sqrt{N}\xi\langle a^\dagger c_p \rangle, \end{aligned} \quad (18f)$$

$$\begin{aligned} \frac{d\langle a^\dagger c_p \rangle}{dt} &= \left(i(\Delta - \delta) - \frac{1}{2}\Gamma\right) \langle a^\dagger c_p \rangle \\ &+ i\sqrt{N}\xi\langle \tilde{e}_0^\dagger c_p \rangle - i\sqrt{N}J\langle a^\dagger \tilde{e}_0 \rangle, \end{aligned} \quad (18g)$$

where $\langle \tilde{e}_k^\dagger \tilde{e}_k \rangle_L$ is defined as

$$\langle \tilde{e}_k^\dagger \tilde{e}_k \rangle_L = \sum_{k \neq 0} \langle \tilde{e}_k^\dagger \tilde{e}_k \rangle. \quad (19)$$

Additionally, $\delta = \omega_p - \omega_d$ is the photon-ring detuning and $\Delta = \omega_a - \omega_d$ is the acceptor-ring detuning, where ω_p is the photon frequency, ω_a is the acceptor frequency, and ω_d the ring-atom frequency. It should be noted that the $k \neq 0$ modes only contribute to the previous set of coupled equations when $\gamma \neq 0$.

We are interested in the transfer efficiency, η , which is the probability that the excitation is transferred to the RC, and is defined as

$$\eta = \int_0^\infty 2\Gamma \langle a^\dagger a(t) \rangle dt. \quad (20)$$

η can be calculated without solving Eqs. (18a)-(18g) explicitly. This is done in Appendix E, where we apply a Laplace transform technique to obtain η . This method works for a linear system without explicit time-dependent coupling constants and with Liouvillian matrix eigenvalues with negative real parts. These conditions are satisfied for this system which has only dissipation and dephasing, but no driving. Starting with a single incident photon, i.e., $\langle c_p^\dagger c_p(0) \rangle = 1$, and using Eq. (D23b) and (E15) we find the transfer efficiency as

$$\eta = \frac{\eta_n}{\eta_d}, \quad (21)$$

where the numerator η_n and denominator η_d in Eq. (21) are defined as

$$\eta_n = \xi^2 \Gamma (\delta_c^2 \gamma \mu \nu - 2\delta_c \Delta_c \gamma \mu \nu + \Delta_c^2 \mu (\gamma \nu + \kappa N \Gamma) + (\gamma \Gamma + \kappa N \nu) (\mu (J^2 N + \nu \Gamma) + N \nu \xi^2)), \quad (22a)$$

$$\begin{aligned} \eta_d &= \delta_c^2 \mu (\kappa \mu \Gamma (\Delta_c^2 + \nu^2) + \nu \xi^2 (\gamma \Gamma + \kappa N \nu)) - 2\delta_c \Delta_c \mu (\kappa \mu \Gamma (\Delta_c^2 - J^2 N + \nu^2) + \nu \xi^2 (\gamma \Gamma + \kappa N \nu)) \\ &+ \Delta_c^2 \mu (\kappa \mu \Gamma (\gamma^2 + 2\kappa(\gamma + \Gamma) + 2\gamma \Gamma - 2J^2 N + \kappa^2 + 2\Gamma^2) + \xi^2 (\kappa N (\gamma^2 + 2\kappa(\gamma + \Gamma) + 2\gamma \Gamma + \kappa^2 + 2\Gamma^2) + \gamma \nu \Gamma)) \\ &+ \Delta_c^4 \kappa \mu^2 \Gamma + \Gamma (\mu (J^2 N + \nu \Gamma) + N \nu \xi^2) (\xi^2 (\gamma \Gamma + \kappa N \nu) + \kappa \mu (J^2 N + \nu \Gamma)), \end{aligned} \quad (22b)$$

where $\delta_c = \delta - 2g$, $\Delta_c = \Delta - 2g$, $\mu = \kappa + \gamma$ and $\nu = \kappa + \gamma + \Gamma$.

C. LH1-RC with Disorder

In the more generalized case where parameters $\omega_{d,j}$ and J_j are site-dependent, we can no longer use the collective Hamiltonian \tilde{H} in Eq. (14). Instead, we employ the Hamiltonian H in Eq. (7) and using Eq. (9) we obtain the set of coupled equations for the following operator averages: $\langle c_p^\dagger c_p \rangle$, $\langle a^\dagger a \rangle$, $\langle e_i^\dagger e_j \rangle$, $\langle e_j^\dagger a \rangle$, $\langle e_j^\dagger c_p \rangle$, and $\langle a^\dagger c_p \rangle$ ($i, j \in [1, N]$),

$$\frac{d\langle c_p^\dagger c_p \rangle}{dt} = i \sum_{i=1}^N J_i (\langle e_i^\dagger c_p \rangle - \langle c_p^\dagger e_i \rangle), \quad (23a)$$

$$\frac{d\langle a^\dagger a \rangle}{dt} = -\Gamma \langle a^\dagger a \rangle + i \sum_{i=1}^N \xi (\langle e_i^\dagger a \rangle - \langle a^\dagger e_i \rangle), \quad (23b)$$

$$\begin{aligned} \frac{d\langle e_i^\dagger e_j \rangle}{dt} = & -(\kappa + \gamma(1 - \delta_{ij}) + i(\delta_i - \delta_j)) \langle e_i^\dagger e_j \rangle \\ & + iJ_i \langle c_p^\dagger e_j \rangle - iJ_j \langle e_i^\dagger c_p \rangle + i\xi (\langle a^\dagger e_j \rangle - \langle a^\dagger c_p \rangle) \\ & + ig(\langle e_{i+1}^\dagger e_j \rangle + \langle e_{i-1}^\dagger e_j \rangle - \langle e_i^\dagger e_{j+1} \rangle + \langle e_i^\dagger e_{j-1} \rangle), \end{aligned} \quad (23c)$$

$$\begin{aligned} \frac{d\langle e_j^\dagger a \rangle}{dt} = & \left(-i\Delta_j - \frac{1}{2}(\gamma + \Gamma + \kappa) \right) \langle e_j^\dagger a \rangle \\ & + i\xi \langle a^\dagger a \rangle + iJ_j \langle c_p^\dagger a \rangle - i\xi \sum_{i=0}^N \langle e_i^\dagger e_i \rangle \\ & + ig(\langle e_{j-1}^\dagger a \rangle + \langle e_{j+1}^\dagger a \rangle), \end{aligned} \quad (23d)$$

$$\begin{aligned} \frac{d\langle e_j^\dagger c_p \rangle}{dt} = & (-i\delta_j - \frac{1}{2}(\gamma + \kappa)) \langle e_j^\dagger c_p \rangle \\ & + iJ_j \langle c_p^\dagger c_p \rangle + i\xi \langle a^\dagger c_p \rangle - i \sum_{i=0}^N J_i \langle e_i^\dagger e_i \rangle \\ & + ig(\langle e_{j-1}^\dagger c_p \rangle + \langle e_{j+1}^\dagger c_p \rangle), \end{aligned} \quad (23e)$$

$$\begin{aligned} \frac{d\langle a^\dagger c_p \rangle}{dt} = & \left(i(\omega_a - \omega_p) - \frac{1}{2}\Gamma \right) \langle a^\dagger c_p \rangle \\ & + i \sum_{i=1}^N \left(\xi \langle e_j^\dagger c_p \rangle - J_i \langle a^\dagger e_j \rangle \right), \end{aligned} \quad (23f)$$

where $\delta_j = \omega_p - \omega_{d,j}$ is the site dependent photon-donor detuning and $\Delta_j = \omega_a - \omega_{d,j}$ is the site dependent acceptor-donor detuning. We can use the method outlined in Appendix E to numerically calculate the transfer efficiency defined in Eq. (20) using the initial condition $\langle c_p^\dagger c_p(0) \rangle = 1$.

Using the k -space collective operators in Eq. (11), we can calculate the probabilities of the k -space population expectations for the system with disorder as

$$\langle \tilde{\mathbf{e}}_k^\dagger \tilde{\mathbf{e}}_k \rangle = \frac{1}{N} \sum_{m=1}^N \sum_{n=1}^N e^{i2\pi k(n-m)/N} \langle e_m^\dagger e_n \rangle. \quad (24)$$

The loss, L_k , for each k -mode from the ring via spontaneous decay is defined as

$$L_k = \int_0^\infty 2\kappa \langle \tilde{\mathbf{e}}_k^\dagger \tilde{\mathbf{e}}_k \rangle dt. \quad (25)$$

It should be noted that the probability-conservation identity $\eta + \sum_{k=0}^{N-1} L_k = 1$, where the transfer efficiency η is defined in Eq. (20).

III. RESULTS

Unless otherwise stated, the following constant parameter values without disorder are $J = 0.1\xi$, $g = 0.3\xi$, $\Gamma = 0.3\xi$, $\kappa = 0.3\xi$, $\omega_a = 12\xi$, $\omega_d = 11.4\xi$, and $\Delta = 0.6\xi$ as in [24].

In the case of disorder, the same parameter values are used, i.e. $\Gamma = 0.3\xi$, $\kappa = 0.3\xi$, $g = 0.3\xi$, and $\omega_a = 12\xi$. We use J_i/ξ ($\omega_{d,i}/\xi$) as normally distributed random variables with mean μ_J (μ_d) and standard deviation σ_J (σ_d).

A. Methods

Our systems contain a set of operators expectation values $\langle O_i(t) \rangle$, $i = 1, \dots, N_0$, with time evolution defined by the equation of motion

$$\frac{dP(t)}{dt} = MP(t), \quad (26)$$

where $P(t) = (\langle O_1(t) \rangle, \dots, \langle O_{N_0}(t) \rangle)^T$ and M is a time independent matrix of dimension $N_0 \times N_0$ with eigenvalues ϵ_i ($i = 1, \dots, N_0$) where $\text{Re}[\epsilon_i] < 0$. For the initial conditions $\langle O_i(0) \rangle = 1$ ($i \in \{1, \dots, N_0\}$) and $\langle O_k(0) \rangle = 0$ ($k \neq i$), in Appendix E we found that

$$\int_0^\infty \langle O_j(t) \rangle dt = (-1)^{i+j+1} \frac{\text{Det}[M_{j,i}^M]}{\text{Det}[M]}, \quad (27)$$

where $M_{j,i}^M$ is the $(j, i)^{th}$ sub-matrix of M . This method is used to calculate the transfer efficiencies η defined in Eq. (20) and the losses L_k defined in Eq. (25). η and L_k were calculated analytically for the ordered system in Sec. II B where $N_0 = 10$ and numerically in Sec. II C for the system with disorder where in general for N donors, $N_0 = N^2 + 4N + 4$.

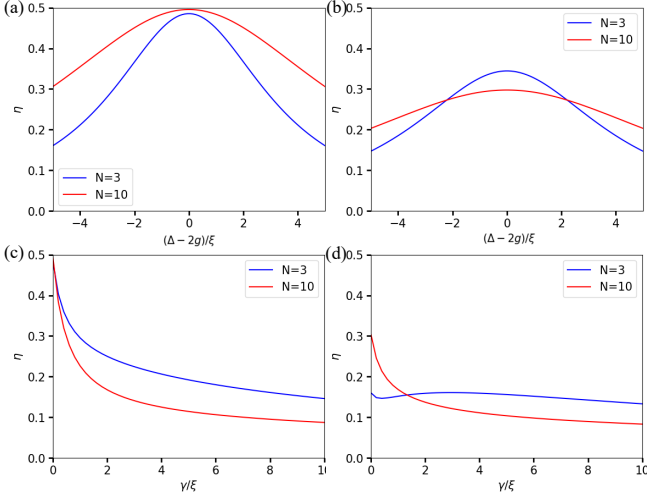


FIG. 2. Plots of the efficiency η_0 in Eq. (28) for the LH1-RC system without light and no disorder. (a) Plots of η_0 against $(\Delta - 2g)/\xi$ for $\gamma = 0$. (b) Plots of η_0 against $(\Delta - 2g)/\xi$ for $\gamma = 0.5\xi$. (c) Plots of η_0 vs γ/ξ with $(\Delta - 2g)/\xi = 0$. (d) Plots of η_0 vs γ/ξ for $(\Delta - 2g)/\xi = 5$. Each figure shows graphs for $N = 3$ (—) and $N = 10$ (—).

B. LH1-RC without Light and no Disorder

We first consider the case without light and no disorder, where the ring has an initial excitation delocalized among the donor atoms. In this case we consider Eqs. (18a)-(18g) with $J = 0$ and the initial conditions $\langle \tilde{\mathbf{e}}_k^\dagger \tilde{\mathbf{e}}_k(0) \rangle = \delta_{0k}$ and $\langle a^\dagger a(0) \rangle = 0$. In this case the analytic form of the efficiency, η_0 , calculated in Appendix E, is as follows

$$\eta_0 = \frac{\xi^2 \Gamma(\gamma + \kappa N)(\gamma + \kappa + \Gamma)}{\kappa \Gamma(\gamma + \kappa) ((\Delta - 2g)^2 + (\gamma + \kappa + \Gamma)^2) + \xi^2(\gamma + \kappa + \Gamma)(\kappa N(\gamma + \kappa + \Gamma) + \gamma \Gamma)}. \quad (28)$$

It should be noted that for $\gamma/\xi = 0$,

$$\eta_0 = \frac{\Gamma N \xi^2 (\Gamma + \kappa)}{(\Delta - 2g)^2 \Gamma \kappa + (\Gamma + \kappa)^2 (\Gamma \kappa + N \xi^2)}. \quad (29)$$

For $(\Delta - 2g)/\xi = 0$

$$\eta_0 = \frac{\xi^2 \Gamma(\gamma + \kappa N)}{\xi^2 (\kappa N(\gamma + \kappa + \Gamma) + \gamma \Gamma) + \kappa \Gamma(\gamma + \kappa)(\gamma + \kappa + \Gamma)}, \quad (30)$$

and for $\kappa = 0$, $\eta_0 = 1$

Figs. 2(a) and 2(b) are plots of η_0 against the dimensionless collective acceptor-ring detuning $(\Delta - 2g)/\xi$, for dimensionless dephasing values $\gamma/\xi = 0$ and $\gamma/\xi = 0.5$, respectively for $N = 3$ (—) and $N = 10$ (—). We observe a decrease in the on-resonance maximum transfer efficiency from 0.485 (0.496) to 0.344 (0.298) for $N = 3$ ($N = 10$) as γ/ξ is increased from $\gamma/\xi = 0$ to $\gamma/\xi = 0.5$. The increase in γ/ξ causes a larger decrease in the maximum transfer efficiency for $N = 10$ compared to $N = 3$. The full-width at half maximum (FWHM) bandwidth of η_0 increases from 7.03 (12.7) to 8.63 (14.7) for $N = 3$ ($N = 10$) as γ/ξ is increased from $\gamma/\xi = 0$ to $\gamma/\xi = 0.5$. When $\gamma/\xi = 0$, η_0 ($N = 10$) $>$ η_0 ($N = 3$) for all values of $(\Delta - 2g)/\xi$. However for $\gamma/\xi = 0.5$, η_0 ($N = 3$) $>$ η_0 ($N = 10$) in the region $|(\Delta - 2g)/\xi| < 2.21$, and η_0 ($N = 10$) $>$ η_0 ($N = 3$) in the region $|(\Delta - 2g)/\xi| > 2.21$.

Figs. 2(c) and 2(d) are plots η_0 against the dimensionless dephasing parameter γ/ξ , for $(\Delta - 2g)/\xi = 0$ and $(\Delta - 2g)/\xi = 5$, respectively. When $(\Delta - 2g)/\xi = 0$, η_0 ($N = 10$) $>$ η_0 ($N = 3$) for $\gamma/\xi < 0.0593$, and η_0 ($N = 3$) $>$ η_0 ($N = 10$) for $\gamma/\xi > 0.0593$. When $(\Delta - 2g)/\xi = 5$, η_0 ($N = 10$) $>$ η_0 ($N = 3$) for $\gamma/\xi < 1.34$ and η_0 ($N = 3$) $>$ η_0 ($N = 10$) for $\gamma/\xi > 1.34$. When there is no detuning, η_0 decreases monotonically with increasing dephasing for both values of N . However, with detuning, η_0 decreases monotonically for $N = 10$, but when $N = 3$, η_0 decreases to a minimum of 0.147 at $\gamma/\xi = 0.193$, followed by an increase to a maximum of 0.161 at $\gamma/\xi = 2.94$, and then decreases monotonically for $\gamma/\xi > 2.94$. A similar behavior of η_0 is observed for larger values of N with larger detuning values.

The key findings are that when there is no dephasing (Eq. (29)), larger N always gives larger efficiencies. On-resonant, it is found that increasing the dephasing leads to a monotonic decrease in the transfer efficiency for arbitrary N . This decrease is found to be less for the off-resonance case. We should note that our simulations indicate that the decrease is more significant for larger values of N . Dephasing couples the $k = 0$ mode to the dissipative $k \neq 0$ modes, which do not couple to the acceptor. For a specific value of $N \in [3, 10]$ if $|(\Delta - 2g)/\xi| \gtrsim 0.508 + 1.20N$, increasing γ/ξ results in a

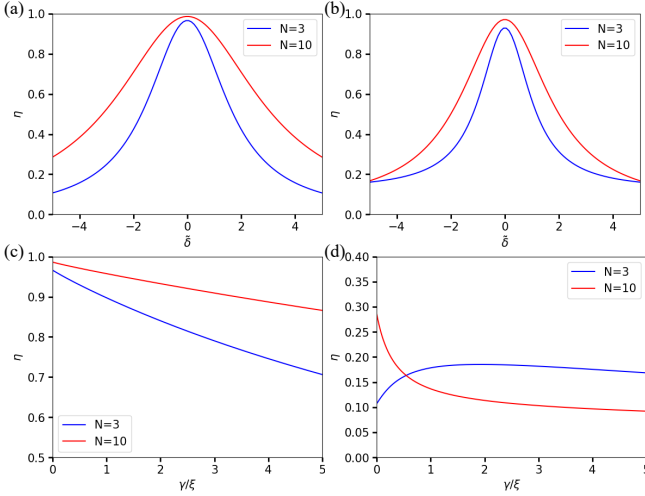


FIG. 3. Plots of the efficiency η in Eq. (21) with an incident photon and no disorder. (a) Plots of η against $\tilde{\delta} = (\delta - \Delta)/\xi$ for $\gamma/\xi = 0$. (b) Plots of η against $\tilde{\delta}/\xi$ for $\gamma/\xi = 0.5$. (c) Plots of η against γ/ξ for $\tilde{\delta} = 0$. (d) Plots of η against γ/ξ for $\tilde{\delta} = 5$. Each figure shows graphs for $N = 3$ (—) and $N = 10$ (—).

minimum and a maximum in the transfer efficiency (see for example Fig. 2(d) for $N = 3$ and $(\Delta - 2g)/\xi = 2.94$), where we find ENAQT.

C. LH1-RC with an Incident Photon and without Disorder

Now we consider the case with an incident photon and no disorder. The initial state has $\langle c_p^\dagger c_p(0) \rangle = 1$, $\langle \tilde{e}_k^\dagger \tilde{e}_k(0) \rangle = 0$, and $\langle a^\dagger a(0) \rangle = 0$, and the transfer efficiency is given in Eq. (21). Figs. 3(a) and 3(b) are plots of η against the dimensionless collective photon-ring detuning, $\tilde{\delta} = (\delta - \Delta)/\xi$, for $\gamma/\xi = 0$ and $\gamma/\xi = 0.5$, respectively. In both cases ($\gamma/\xi = 0$ and $\gamma/\xi = 0.5$) we observe a maximum in the transfer efficiency for $N = 3$ and $N = 10$ at $\tilde{\delta}/\xi = 0$. We observe a small decrease in the on-resonance maximum from 0.966 (0.986) to 0.923 (0.971) for $N = 3$ ($N = 10$), as dephasing increases from $\gamma/\xi = 0$ to $\gamma/\xi = 0.5$. We also observe that the bandwidth decreases from 3.53 (6.38) to 2.59 (4.13) for $N = 3$ ($N = 10$), as dephasing increases. Without dephasing η ($N = 10$) $>$ η ($N = 3$) for all values of $\tilde{\delta}$, however, with dephasing, η ($N = 10$) $>$ η ($N = 3$) for $|\tilde{\delta}| < 5.25$ and η ($N = 10$) $<$ η ($N = 3$) for $|\tilde{\delta}| > 5.25$.

Figs. 3(c) and 3(d) are plots of η against the dimensionless dephasing parameter γ/ξ , for $\tilde{\delta} = 0$ and $\tilde{\delta} = 5$, respectively. We observe that for the no detuning case, η ($N = 10$) $>$ η ($N = 3$) for all values of γ/ξ . However, when the detuning is non-zero, η ($N = 10$) $>$ η ($N = 3$) occurs in the range $\gamma/\xi < 0.546$, and η ($N = 10$) $<$ η ($N = 3$) occurs in the range $\gamma/\xi > 0.546$. Similar to

the case without light, increasing γ/ξ causes a decrease in the on-resonance efficiency for all N , however, with detuning, we observe that for $N = 3$ there is a maximum efficiency of 0.185 at $\gamma/\xi = 1.92$. We find that for $\tilde{\delta} = 0$, the efficiency scales with γ approximately as

$$\eta(\gamma) \approx \frac{200(5\gamma(N+1) + 3N)}{10\gamma(30\gamma + 101N + 127) + 9(67N + 6)}. \quad (31)$$

$\eta(\gamma)$ has an FWHM of approximately $\frac{50N^2 + 46N + 9}{15N}$. Off-resonance, numerical calculations show that when $\tilde{\delta} \gtrsim 1.43 + 0.85N$, there is a dephasing value $\gamma/\xi > 0$ which maximizes the transfer efficiency. When $\tilde{\delta} \gg 1.43 + 0.85N$, we find an approximation for the transfer efficiency as

$$\eta(\gamma) \approx \frac{500\gamma}{5\gamma(30\gamma + 100N + 127) + 300N + 27}. \quad (32)$$

Comparing the LH1-RC system without light to the system with an incident photon, we observe significantly higher transfer efficiencies in the latter case. For example, for $N = 3$, the on-resonance maximum is 0.986 with an incident photon, and 0.486 without light. We also observe that dephasing decreases the maximum transfer efficiency of the system without light more significantly than the system with an incident photon.

D. LH1-RC with an Incident Photon and Disorder in the Energetics and Photon-Ring Coupling Constants

Figs. 4(a) and 4(b) (Figs. 4(c) and 4(d)) are plots of η against the dimensionless photon-acceptor detuning, $\tilde{\delta} = (\delta - \Delta)/\xi$, for constant donor-atom onsite energy $\omega_{d,i} = g = 11.4\xi$ and disorder in the photon-ring coupling J_i/ξ for $N = 3$ ($N = 10$), with $\gamma/\xi = 0$ and $\gamma/\xi = 0.5$, respectively. We use J_i/ξ as a normally distributed random variable with mean $\mu_J = 0.1$ and standard deviations $\sigma_J = 0$ (—) and $\sigma_J = 0.005$ (—). η is then calculated using the method in Appendix E for 100 trials to obtain an average value of η , with error bars of one standard deviation of the sample using the central limit theorem. For $N = 3$ there is no significant effect of the photon-ring disorder on the transfer efficiency with and without dephasing. The dephasing has the same effect of reducing the FWHM as in the no-disorder case (see Figs. 3(a) and 3(b)). For $N = 10$, with no dephasing, disorder reduces η for $\tilde{\delta} \in [-2, 1.8]$, while for $\gamma/\xi = 0.5$, η is reduced for $\tilde{\delta} \in [-1.9, 1.4]$. The percentage change on resonance due to disorder is 24.4% without dephasing, and 15.4% with dephasing. The reduction in η is therefore less significant with dephasing. The decrease in efficiency due to disorder is explained by the increased coupling of the photon mode to the $k \neq 0$ excitonic modes on the ring, which leads to greater dissipation from the ring, thus lowering the efficiency. Dephasing reduces the

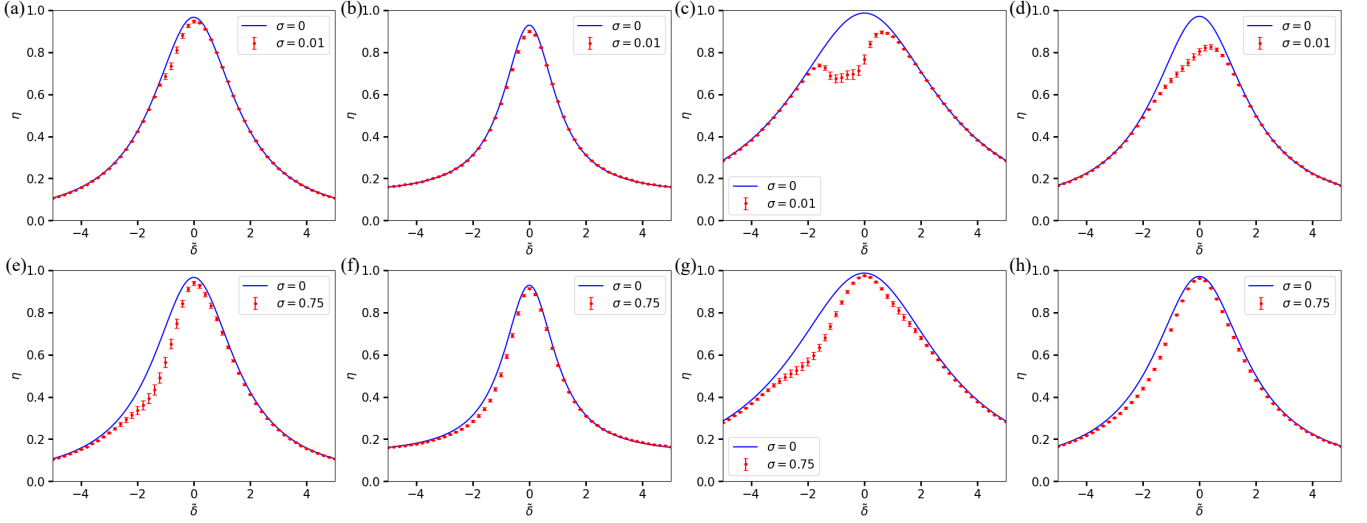


FIG. 4. Plots of the efficiency η for the LH1-RC system with an incident photon and disorder. Figs 4(a) and 4(b) are plots of η against $\tilde{\delta} = (\delta - \Delta)/\xi$ for no disorder (—) and disorder in J_i/ξ (---) with error bars using $\gamma/\xi = 0$ and $\gamma/\xi = 0.5$, respectively for $N = 3$. Figs 4(c) and 4(d) are plots of η against $\tilde{\delta}$ for no disorder (—) and disorder in J_i/ξ (---) with error bars for $\gamma/\xi = 0$ and $\gamma/\xi = 0.5$, respectively for $N = 10$. Figs 4(e) and 4(f) (4(g), and 4(h)) are plots of η against $\tilde{\delta}$ for no disorder (—) and disorder in $\omega_{d,i}/\xi$ (---) with error bars for $N = 3$ ($N = 10$) with $\gamma/\xi = 0$ and $\gamma/\xi = 0.5$, respectively.

negative effect of disorder on the transfer efficiency, because it couples the $k \neq 0$ modes to the $k = 0$ mode which increases coupling to the acceptor. However, without dephasing the $k \neq 0$ modes do not couple to the acceptor and therefore increased dissipation of the excitation from the ring occurs. A more detailed graphical demonstration of dissipation is given in Fig. 5(a) and 5(b).

Figs. 4(e) and 4(f) (4(g) and 4(h)) are plots of η against $\tilde{\delta}$ for no disorder in J_i ($J_i = 0.1\xi$) and disorder in $\omega_{d,i}/\xi$ for $N = 3$ ($N = 10$), with $\gamma/\xi = 0$ and $\gamma/\xi = 0.5$, respectively. We use $\omega_{d,i}/\xi$ as a normally distributed random variable with mean $\mu_{\omega_d} = 11.4$ and standard deviations $\sigma_{\omega_d} = 0$ (—) and $\sigma_{\omega_d} = 0.75$ (---). Without dephasing for $N = 3$ and $N = 10$, we find a decrease in transfer efficiency in regions away from resonance, with the decrease being more significant $\tilde{\delta} < 0$. With dephasing, we find that disorder in $\omega_{d,i}$ has a negligible effect on the transfer efficiency for all detunings.

We note that disorder in the parameters g , γ , and κ had no effect on the transfer efficiency regardless of other parameter values and disorder strengths. Disorder in ξ caused a decrease in the transfer efficiency equivalent to disorder in J_i .

Figs. 5(a) and 5(b) are plots of the mode losses, L_k , defined in Eq. (25) for each mode $k = 0, \dots, 9$, against the dimensionless detuning $\tilde{\delta}$ for $N = 10$, $\omega_{d,i}/\xi = 11.4$ and normally distributed disorder in J_i/ξ ($\mu_J = 0.1$ and $\sigma_J = 0.01$), for $\gamma/\xi = 0$ and $\gamma/\xi = 1$, respectively. η is calculated for 100 trials to obtain an average, with error bars of one standard deviation of the sample using the central limit theorem. Plots are shown for L_0 (—), $L_1 = L_9$ (—), $L_2 = L_8$ (—), $L_3 = L_7$ (—), $L_4 = L_6$ (—) and L_5 (—).

In Fig. 5(a), $L_0 = 1 - \eta$, where η is the efficiency plotted in Fig. 4(c) in the no-disorder case with no dephasing (—). L_0 therefore represents the total loss of the excitation from the ring in the no-disorder and no-dephasing case. $\sum_{k=0}^9 L_k = 1 - \eta$, where η is the efficiency plotted in Fig. 4(c) in the disorder in J_i/ξ case with no dephasing (—). Therefore, in the case with disorder, $\sum_{k=0}^9 L_k$ represents the total loss of the excitation from the ring. It should be noted that in the case with disorder and no dephasing, the k -modes are only coupled to the photon. In addition, the maxima of the various loss terms L_k occur at the following detuning values: $\tilde{\delta} = -1.2$ for L_5 ; $\tilde{\delta} = -1.1$ for L_4 and L_6 ; $\tilde{\delta} = -0.8$ for L_3 and L_8 ; $\tilde{\delta} = -0.4$ for L_2 and L_8 ; and $\tilde{\delta} = -0.1$ for L_1 and L_9 .

In Fig. 5(b), with dephasing $\gamma/\xi = 1$, the mode losses L_k ($k = 1, \dots, 9$) have reduced maxima in the range $-2 \leq \tilde{\delta} \leq 2$ compared to the same losses in Fig. 5(a) without dephasing. With disorder and dephasing, each k -mode is coupled to the photon and all the other k -modes. This leads to a redistribution of losses over the various modes and a flattening of the mode loss terms L_k ($k = 1, \dots, 9$). It should be noted that without disorder L_k for $k \neq 0$ are all equal (see Eq (D24) in Appendix D).

Fig. 5(c) gives plots of the dimensionless eigenenergy $\tilde{\epsilon}_2 = (\epsilon_2 - \omega_d)/\xi$ (—) against the dimensionless photon-acceptor detuning $\tilde{\delta}$, for the coupled system without disorder described by the Hamiltonian \tilde{H}_c in Eq. (15a). The dimensionless eigenenergies, $\tilde{\omega}_k = (\omega_k - \omega_d)/\xi$ ($k = 1, \dots, 9$), of the decoupled system described by the Hamiltonian \tilde{H}_D in Eq. (15b) are given by the horizontal lines: $\tilde{\omega}_5 = -0.600$ (—), $\tilde{\omega}_4 = \tilde{\omega}_6 = -0.485$ (—), $\tilde{\omega}_3 = \tilde{\omega}_7 = -0.185$ (—), $\tilde{\omega}_2 = \tilde{\omega}_8 = 0.185$ (—), and $\tilde{\omega}_1 = \tilde{\omega}_9 = 0.485$ (—). The eigenenergy $\tilde{\epsilon}_2$ coincides

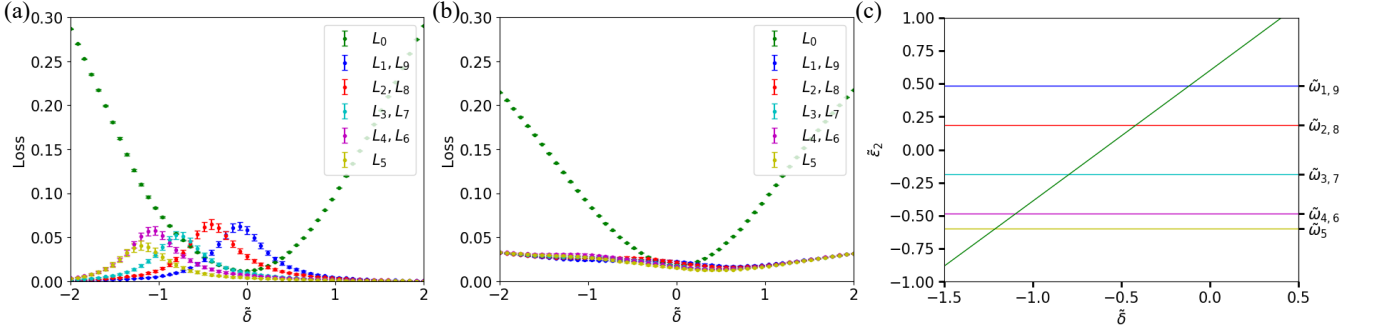


FIG. 5. LH1-RC system with an incident photon for $g/\xi = 0.3$ and $N = 10$. (a) and (b) are plots of loss, L_k in Eq. (25) with error bars against detuning $\tilde{\delta} = (\delta - \Delta)/\xi$, of collective k -modes ($k = 0, \dots, 9$) where J_i/ξ is a normally distributed random variable with $\mu_J = 0.1$ and $\sigma_J = 0.01$, for $\gamma/\xi = 0$ and $\gamma/\xi = 1$, respectively. Figs. 5(a) and 5(b) show the losses L_0 (—), $L_1 = L_9$ (—), $L_2 = L_8$ (—), $L_3 = L_7$ (—), $L_4 = L_6$ (—) and L_5 (—). (c) Eigenvalue $\tilde{\epsilon}_2$ of the coupled Hamiltonian \tilde{H}_c in Eq. (16) (—) against photon-acceptor detuning $\tilde{\delta}$. The decoupled energies, $\tilde{\omega}_k = (\omega_k - \omega_d)/\xi$ ($k = 1, \dots, 9$), in Eq. (15b) are marked horizontally.

with the eigenenergies $\tilde{\omega}_k$, at the following dimensionless detuning values: $\tilde{\epsilon}_2 = \tilde{\omega}_5$ at $\tilde{\delta} = -1.21$; $\tilde{\epsilon}_2 = \tilde{\omega}_{4,6}$ at $\tilde{\delta} = -1.10$; $\tilde{\epsilon}_2 = \tilde{\omega}_{3,7}$ at $\tilde{\delta} = -0.794$; $\tilde{\epsilon}_2 = \tilde{\omega}_{2,8}$ at $\tilde{\delta} = -0.419$; and $\tilde{\epsilon}_2 = \tilde{\omega}_{1,9}$ at $\tilde{\delta} = -0.116$. These detuning values are approximately equal to the detuning values of the respective peaks in each L_k of Fig. 5(a).

The effect of disorder in J_i introduces the coupling of the decoupled modes of the ring to the photon and these modes decay via spontaneous emission from the ring. The additional coupling of the decoupled modes therefore reduces the transfer efficiency of the system in the detuning range $-2 \leq \tilde{\delta} \leq 1.8$ in Fig. 4(c). This corresponds to the detuning range over which losses occur as shown in Fig. 5(a). The decay of the excitation from the ring via the decoupled modes is greatest when $\tilde{\omega}_k = \tilde{\epsilon}_2$, i.e. when the energy of the decoupled mode equals the energy of the first excited state of the collective system. Since L_0 is mostly unaffected by disorder, the additional decay channels of the excitation from the donor via the $k \neq 0$ modes decreases the transfer efficiency of the excitation.

In the case of disorder in the energies $\omega_{d,i}$, the detuning range in which disorder affects the transfer efficiency suggests a similar mechanism as in the case with disorder in J_i . However, instead of additional coupling between the photon and $k \neq 0$ modes, we find additional coupling between the $k = 0$ and $k \neq 0$ modes, when $\tilde{\epsilon}_2 \approx \tilde{\omega}_k$. The new channels created by the disorder will only effect the transfer efficiency provided that the donor-ring is sufficiently populated. However, close to resonance, we find a dark-state mechanism whereby the excitation bypasses the ring and thus the disorder in $\omega_{d,i}$ has a negligible effect. We note that the new coupling caused by onsite energetic disorder is similar to that caused by dephasing.

Fig. 6 are plots of the transfer efficiencies for the system with $N = 10$, $\tilde{\delta} = 0$, $\omega_{d,i} = \omega_d$, and J_i/ξ normally distributed with $\mu_J = 0.1$ and $\sigma_J = 0.01$. η is calculated for 100 trials to obtain an average, with error bars of one

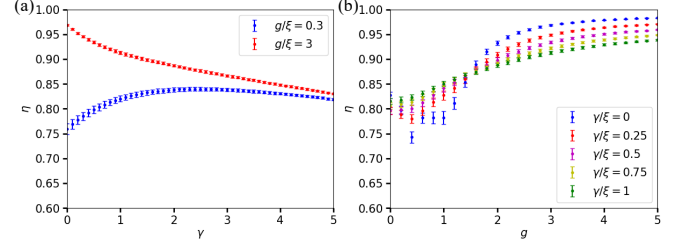


FIG. 6. LH1-RC system with an incident photon with disorder, for $N = 10$, $\tilde{\delta} = 0$, $\omega_{d,i} = \omega_d$ and J_i/ξ normally distributed with $\mu_J = 0.1$ and $\sigma_J = 0.01$. (a) Efficiency η against dephasing γ/ξ with error bars for $g/\xi = 0.3$ (—) and $g/\xi = 3$ (—). (b) Efficiency η against intra-ring coupling g/ξ with error bars for $\gamma/\xi = 0$ (—), $\gamma/\xi = 0.25$ (—), $\gamma/\xi = 0.5$ (—), $\gamma/\xi = 0.75$ (—) and $\gamma/\xi = 1$ (—).

standard deviation of the sample using the central limit theorem. Fig. 6(a) are plots of the efficiency η against the dimensionless dephasing γ/ξ for $g/\xi = 0.3$ (—) and $g/\xi = 3$ (—). We see for $g/\xi = 3$, the efficiency has a maximum of $\eta = 0.972$ at $\gamma/\xi = 0$, and monotonically decreases as γ/ξ increases. When $g/\xi = 0.3$, as γ/ξ increases, η initially increases to a maximum of $\eta = 0.840$ at $\gamma/\xi = 2.5$, followed by a slight monotonic decrease. Fig. 6(b) are plots of the efficiency η against intra-ring coupling g/ξ for $\gamma/\xi = 0$ (—), $\gamma/\xi = 0.25$ (—), $\gamma/\xi = 0.5$ (—), $\gamma/\xi = 0.75$ (—) and $\gamma/\xi = 1$ (—). We see that for $\gamma/\xi = 0$, there is an initial decrease to a minimum of $\eta = 0.743$ at $g/\xi = 0.4$, followed by a monotonic increase. However, for $\gamma/\xi = 1$, η monotonically increases as g/ξ increases. η ($\gamma/\xi = 1$) $>$ η ($\gamma/\xi = 0$) in the range $0 \leq g/\xi < 1.5$, and η ($\gamma/\xi = 1$) $<$ η ($\gamma/\xi = 0$) for $g/\xi > 1.5$. In general, when $g/\xi \leq 1.5$ an increase in γ/g leads to an increase in the transfer efficiency, however when $g/\xi > 1.5$ an increase in γ/ξ leads to a decrease in the transfer efficiency.

In general, when g/ξ increases, $|\tilde{\omega}_k|$ increases and

$\tilde{\omega}_k = \tilde{\epsilon}_i$ occurs at larger values of $|\tilde{\delta}|$, away from the on-resonance value (see Fig. 4(c)). The value of $\tilde{\delta}$ when $\tilde{\omega}_k = \tilde{\epsilon}_i$ gives the strongest coupling between the photon and the dissipative k -modes of the ring. This means that the photon and the dissipative k -modes would have an increasingly weaker coupling at $\tilde{\delta} = 0$ as g/ξ increases, leading to higher transfer efficiencies, which is observed generally in Fig. 6(b). In the no-dephasing case, the $k \neq 0$ modes are purely dissipative, so when g/ξ increases, this leads to higher efficiencies at $\tilde{\delta} = 0$. In the case with dephasing, the $k \neq 0$ modes couple to the $k = 0$ mode, which is coupled to the acceptor. When g/ξ is small, the coupling between the photon and the $k \neq 0$ modes is large and dephasing will increase transfer of the excitation to the acceptor. Therefore increasing the dephasing strengthens the coupling between the $k \neq 0$ modes and $k = 0$ mode thus lowering the population on the dissipative modes, leading to an increase in the transfer efficiency. When g/ξ is large, the coupling between the photon and the $k \neq 0$ modes is small and dephasing reduces the transfer efficiency. Increasing dephasing strengthens the coupling between the $k = 0$ mode to the dissipative k -modes, which decreases the transfer efficiency. We see this in Fig. 6(b), where $g/\xi < 1.5$, dephasing has a positive effect on the transfer efficiency, but when $g/\xi > 1.5$, it has a negative effect on the transfer efficiency.

We note for general N , with $J/\xi \leq 0.1$, $\epsilon_2 \approx \omega_d + \delta$. Since $\omega_k = \omega_d + 2g \cos(2\pi k/N)$, disorder will decrease the transfer efficiency if $\delta \approx 2g \cos(2\pi k/N)$ ($k = 1, \dots, N-1$). In addition, we note that optimal transfer efficiency occurs at $\delta \approx \Delta$. If $|\Delta/\xi| \gtrsim 2$ and we choose $g/\xi \ll 1$ then $\delta \gg 2g \cos(2\pi k/N)$ and η is unaffected by disorder. For $|\Delta/\xi| < 2$, η will be unaffected by disorder when $\Delta \ll \min[2g \cos(2\pi k/N)]$, which is most optimal when $N = 4m + 2$ ($m = 1, 2, \dots$). In this case, $\min[2g \cos(2\pi k/N)] = 2g \sin \pi/N$, and we can let $g/\xi \gg \Delta/(2g \sin(\pi/N))$.

E. The Dark-State Mechanism in the LH1-RC System with an Incident Photon

Fig. 7 shows plots for the case with no disorder and no dephasing. Fig. 7(a) gives the plot for the ratio of the eigenvalue with the second smallest magnitude of its real part to the eigenvalue with the smallest magnitude of its real part obtained from the matrix in Eq. D23b against $\tilde{\delta}$. The set of eigenvalues all have negative real parts which results in exponential decay of the populations on the ring and acceptor. This is done for $N = 3$ (—), $N = 10$ (—), $N = 16$ (—), and $N = 32$ (—). An eigenvalue which has a smaller magnitude for its real part would give a longer decay time for the populations. The plots in Fig. 7(a) have maxima of 52.2, 51.2, 51.0, and 50.9 at $\tilde{\delta} = 0$, for $N = 3, 10, 16$, and 32, respectively. When the ratio is large, the eigenvalue whose real part has the smaller magnitude determines the long-time behavior of the populations. When the ratio is small, the long-time

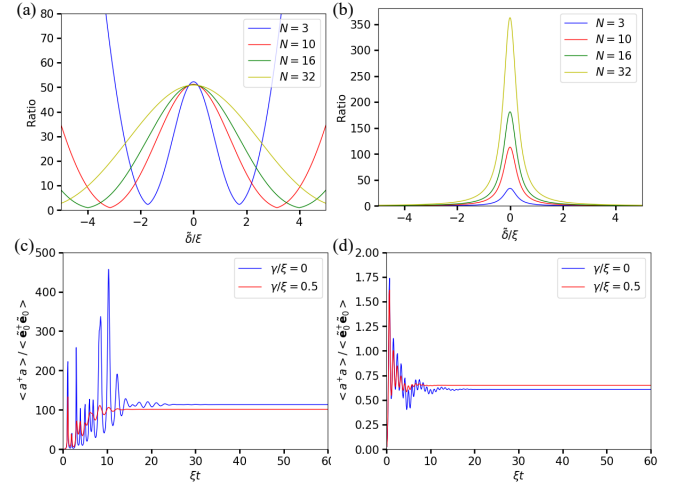


FIG. 7. (a) Plot of the ratio of the eigenvalue with the second smallest magnitude of its real part to the eigenvalue with the smallest magnitude of its real part obtained from the matrix in Eq. D23b against $\tilde{\delta}$. (b) Plot of the population ratio $\langle a^\dagger a \rangle / \langle \tilde{e}_0^\dagger \tilde{e}_0 \rangle$ against $\tilde{\delta}$ for the eigenvector with eigenvalue whose real part has the smallest magnitude. (a) and (b) are plotted for $N = 3$ (—), $N = 10$ (—), $N = 16$ (—), and $N = 32$ (—). (c) and (d) are plots of the population ratio $\langle a^\dagger a \rangle / \langle \tilde{e}_0^\dagger \tilde{e}_0 \rangle$ for $N = 10$ with $\gamma/\xi = 0$ (—) and $\gamma/\xi = 0.5$ (—) against ξt for $\tilde{\delta} = 0$ and $\tilde{\delta} = 4$, respectively.

behavior is determined by multiple eigenvalues.

Fig. 7(b) are plots of the population ratio $\langle a^\dagger a \rangle / \langle \tilde{e}_0^\dagger \tilde{e}_0 \rangle$ against $\tilde{\delta}$ for the eigenvector with eigenvalue whose real part has the smallest magnitude for $N = 3$ (—), $N = 10$ (—), $N = 16$ (—), and $N = 32$ (—). We see that this ratio has maxima of 34.0, 113, 181, and 362 at $\tilde{\delta} = 0$ for $N = 3, 10, 16$, and 32 respectively. Therefore these results indicate that when $\tilde{\delta}$ is small, the long-time dynamics is described by a dark-state, where the excitation probability on the ring is much less than the acceptor. The excitation therefore circumvents the dissipative ring, which reduces loss by spontaneous decay, which results in a high transfer efficiency. For larger N , we find that $\langle a^\dagger a \rangle / \langle \tilde{e}_0^\dagger \tilde{e}_0 \rangle \gg 1$ is satisfied for a larger range of detuning values. For example, when $N = 32$, we find $\langle a^\dagger a \rangle / \langle \tilde{e}_0^\dagger \tilde{e}_0 \rangle \geq 10$ for $|\tilde{\delta}| < 1.78$, however when $N = 3$, $|\tilde{\delta}| < 0.46$. This explains why simulations show that the bandwidth of η monotonically increases with N as is also shown in Fig. 3(a). It should be noted that Wyke et al. [34] found in the perturbative limit ($J/\xi \ll 1$) for $\tilde{\delta} = 0$,

$$\langle a^\dagger a \rangle / \langle \tilde{e}_0^\dagger \tilde{e}_0 \rangle = \frac{N}{(\kappa/\xi)^2}, \quad (33)$$

which for $N = 10$ and $\kappa/\xi = 0.3$ gives $\langle a^\dagger a \rangle / \langle \tilde{e}_0^\dagger \tilde{e}_0 \rangle =$

111, with the following dark-state

$$|\psi\rangle \propto e^{-\frac{\sqrt{2}JN\xi}{\kappa^2 + N\xi^2}t}(|P\rangle - \frac{iJ\kappa\sqrt{N}}{\kappa^2 + N\xi^2}|R\rangle - \frac{JN\xi}{\kappa^2 + N\xi^2}|A\rangle), \quad (34)$$

for $|P\rangle$, $|R\rangle$, and $|A\rangle$ being the excited state of the photon, collective ring and acceptor, respectively. Therefore the dark-state mechanism explains the high transfer efficiency in the system using the phenomenological approach and the Lindblad approach.

Fig. 7(c) and Fig. 7(d) are plots of the population ratio $\langle a^\dagger a \rangle / \langle \tilde{e}_0^\dagger \tilde{e}_0 \rangle$ for $N = 10$ with $\gamma/\xi = 0$ (—) and $\gamma/\xi = 0.5$ (—) against ξt for $\tilde{\delta} = 0$ and $\tilde{\delta} = 4$, respectively. In Fig. 7(c), after initial oscillations, $\langle a^\dagger a \rangle / \langle \tilde{e}_0^\dagger \tilde{e}_0 \rangle$ is 113 and 110 for $\gamma/\xi = 0$ and $\gamma/\xi = 0.5$, respectively. The dephasing has a negligible effect on the ratio and hence the dark-state is preserved such that the system maintains a high transfer efficiency. In Fig. 7(d) the long-time population ratios are 0.608 and 0.649 for $\gamma/\xi = 0$ and $\gamma/\xi = 0.5$, respectively. When $|\tilde{\delta}| \gg 0$ the dark-state is destroyed and the excitation no longer circumvents the dissipative ring which leads to a decreased efficiency.

IV. EXACTLY SOLVABLE MODELS AS AN INTERPRETIVE SCAFFOLD FOR THE NUMERICS

We can give a reduced description of the full LH1-RC system for which the key dynamical quantities can be obtained in closed form, without large-scale numerics. These models reduce the physics down to the essential couplings while preserving the mechanisms of interest (coupling to light, transfer to the acceptor, and losses). Because they are analytic, they tell us *why* a given numerical trend must occur and give us clean baselines to test our code against.

The LH1 ring supports collective excitations (normal modes) labelled by a wave number k . Only the fully symmetric mode ($k = 0$), often called the *bright* mode, couples directly to both the incident photon and the acceptor. All other modes ($k \neq 0$) are *dark*: in the ideal symmetric limit they neither absorb light nor feed the acceptor. This bright/dark decomposition is the central simplification that makes an exact reduction possible.

Projecting the full system onto the bright subspace yields a three-state “trimer”: (photon) \leftrightarrow (bright ring mode) \leftrightarrow (acceptor). The dark modes are decoupled spectators in the ordered (perfectly symmetric) case. This trimer admits closed-form expressions for the steady transfer efficiency to the acceptor, its line shape as a function of detuning, and its dependence on dephasing. In practice, this trimer is the analytic backbone we use to interpret the full simulations. See Appendix B for details.

A. What the solvable core predicts (and how it guides us)

- **Tall resonant peak.** When the photon is tuned to the bright–acceptor resonance, the model predicts a large transfer efficiency. This fixes where the main peak *should* sit in the numerics and how tall it can be.
- **Bandwidth narrowing with dephasing.** Adding moderate dephasing reduces the height and narrows the width of the resonant peak: coherence is partially lost, but the bright pathway still dominates. This is a stringent check on the dephasing implementation.
- **Probability bookkeeping.** In the trimer reduction, efficiency η plus all loss channels L_k sum to one, $\eta + \sum_k L_k = 1$. This identity is a powerful unit test: if a solver violates it, something is off in the Liouvillian, the rates, or the integrator.

B. From coherence to ENAQT (why noise can help off resonance)

Purely coherent dynamics can produce destructive interference that traps population in dark superpositions (“coherent trapping”). Away from resonance, *moderate* environmental dephasing breaks this symmetry just enough to let population reach the acceptor, causing a characteristic *non-monotonic* dependence of efficiency on dephasing (a dip then recovery). This is the standard signature of ENAQT. On resonance, by contrast, dephasing is mostly disadvantageous: it mixes bright into dark modes and lowers the peak.

C. Disorder as controlled bright–dark mixing

Static disorder modifies three things. (i) *Photon–ring coupling disorder* spoils the perfect symmetry by which the photon drives only the bright mode; it leaks amplitude into dark modes that carry loss, especially at detunings where a dark-mode energy crosses a coupled eigenenergy. In numerics this appears as a drop in efficiency and peaks in mode-resolved losses $L_k(\delta)$. (ii) *Energetic disorder* breaks the symmetry and couples the bright mode to the dark modes causing a leakage in amplitude to the dark modes thereby reducing efficiency. Close to resonance the dark state dominates and creates a system which is robust against energetic disorder. (iii) *Intra-ring coupling disorder* perturbs the dark spectrum but, in typical ranges, has a smaller effect on efficiency because it does not strongly change how light addresses bright vs. dark subspaces. The solvable picture makes both trends transparent.

Exactly solvable reductions (ESR) are more than pedagogical since they provide target curves (peak position, height, and width; monotonic vs. non-monotonic trends with dephasing) that the numerical solver must reproduce in the ordered limit before adding complications. ESR discriminate which features come from the *bright* highway to the acceptor and which arise when population leaks into *dark* ‘side streets’. This is how we diagnose dark-state transfer vs. ordinary hopping. We can understand how efficiency scales with detuning, dephasing, ring size, and couplings. This is useful for predicting where peaks/dips should move when a parameter is changed. When full simulations deviate from analytic slopes, limits, or conservation, we have a clear starting point to find either the bug or identify a regime change.

V. CONCLUSION

This paper considered the effects of dephasing and static disorder on an artificial model of the LH1-RC photosynthetic system using a Lindblad master equation approach. The understanding of the effects of dephasing and disorder on transfer efficiencies in artificial photosynthetic light-harvesting systems is crucial for the design of highly-efficient scalable solar energy devices. Dephasing studies can be utilized to improve excitation transfer via ENAQT, which is counteracted by disorder.

We considered transfer efficiencies and a transfer mechanism utilizing a dark-state channel in the LH1-RC light-harvesting system without light and with an incident single photon. Initially, we modeled the no-disorder system with and without dephasing using the collective states of the donor-ring to analytically derive the transfer efficiencies. Then by treating the photon-donor and intra-donor couplings as normally distributed random variables, we numerically obtained the transfer efficiencies with disorder.

We found that with no disorder, no dephasing, and on-resonance, transfer efficiencies of approximately 50% were found without light, however with an incident photon the peak efficiency was over 98%. The effect of dephasing causes a significant decrease of the transfer efficiency to 34% without light, however the transfer efficiency remained high at 97% with an incident photon. Large efficiencies with the incident photon are due to a dark-state type mechanism, where the excitation circumvents the dissipative ring, which reduces loss by spontaneous decay.

Increasing the photon-acceptor detuning causes a sharp fall-off to the transfer efficiency in all cases. We found that for large detunings, the effect of adding dephasing increases the transfer efficiencies. Thus, significant ENAQT occurs in a detuning region far off-resonance.

We found that diagonal on-site disorder on the donor-ring caused a slight decrease in the transfer efficiency away from resonance, which indicates that the dark-state

mechanism is robust against energetic disorder. However, photon-ring coupling disorder caused a significant decrease in the transfer efficiencies for certain values of the photon-acceptor detuning. Disorder has the effect of coupling the dissipative decoupled modes of the donor-ring to the photon, provided these modes have similar eigenenergies to the LH1-RC system. By increasing the intra-ring coupling strength, we can change the decoupled mode eigenenergies so that the reduction in efficiency due to disorder occurs at different detuning values, away from resonance. We found that disorder in the intra-ring coupling and donor-atom dissipation and dephasing had a negligible effect on the transfer efficiency.

In conclusion, we have investigated the effects of dephasing and disorder on the large transfer efficiency for the artificial LH1-RC system. The conditions that lead to large transfer efficiencies occur on-resonance with negligible effect of intra-ring coupling disorder. Photon-ring disorder creates extra dissipative channels in the system due to the coupling of dissipative decoupled ring modes to the photon. However increasing the intra-ring coupling reduces the effect of the dissipative decoupled modes on the transfer efficiency. Dephasing enhances the transfer efficiency far away from resonance, but has a negligible effect on the transfer efficiency close to resonance. The numerical trends reported here follow naturally from a minimal V -system mechanism—two donor superpositions feeding a single acceptor/sink—obtained either by truncating the ring to a representative donor dimer (A, B) plus the acceptor C (with bright/dark superpositions $|\pm\rangle$), or by coarse-graining the full ring into a *bright* collective state $|B_0\rangle$, an effective *dark* state $|D\rangle$, and the acceptor C . In both viewpoints, only the bright channel couples directly to the acceptor, while the dark channel is decoupled in the symmetric, noise-free limit; moderate dephasing mixes dark back into bright (ENAQT), and static asymmetries or disorder inject amplitude into dark, opening loss channels. This is exactly the mechanism we observe in the full ring simulations with dissipation and disorder. In the ordered system a symmetric optical drive excites the bright channel exclusively, yielding a near-unity transfer efficiency on resonance. Adding dephasing reduces coherent selectivity and mixes population into lossy dark pathways, narrowing and slightly lowering the peak. In the V -model this corresponds to conduction through $|+\rangle \leftrightarrow C$ while $|-\rangle$ traps unless mixed by noise. Far from resonance, purely coherent dynamics suppress transfer; moderate dephasing breaks destructive interference and restores flow to the acceptor, producing the non-monotonic efficiency versus dephasing (a dip then recovery) that we report. This is the canonical ENAQT behavior of the V -system.

Drive-side disorder (non-uniform photon-ring coupling) is the V -model analog of pumping both bright and dark channels: it mixes the input into dark states that do not feed the acceptor and instead dissipate on the ring, reducing efficiency over a detuning window. Mode-resolved loss spectra peak where the dressed

bright-acceptor eigenenergy crosses dark-mode energies, confirming this mechanism. By contrast, randomizing intra-ring couplings perturbs the dark spectrum but leaves bright/dark addressing largely intact in the explored range, so the impact on efficiency is much smaller. In the V -language, g sets the bright-dark energy splitting; increasing g pushes dark levels away from the dressed bright-acceptor energy at the operating detuning, reducing resonant leakage into dark and restoring the on-resonance peak. This explains the observed recovery of performance when g is increased. In the symmetric, single-excitation, narrowband regime, the ring reduces exactly to a photon-bright-acceptor trimer, from which closed-form efficiency line shapes and a probability-conservation identity $\eta + \sum_k L_k = 1$ follow. We use these expressions to benchmark the simulations and to predict the location and height of the resonant peak and its dephasing-induced narrowing. A minimal three-state V toy model additionally reproduces coherent trapping and its relief by moderate dephasing.

The V -model provides *quantitative* support in the ordered, single-excitation, narrowband limit (where the trimer reduction is exact), and *qualitative* yet predictive guidance with moderate dephasing and weak-to-moderate disorder. For strong disorder, broadband drives, or multi-excitation dynamics, the V -model remains a reliable guide to the *direction* of effects—bright/dark balance, ENAQT onset, and g -based mitigation—while the full ring numerics supply the needed quantitative detail. Taken together, the V -model perspective explains why we observe (i) a near-unity resonant peak that narrows under dephasing, (ii) ENAQT off resonance, (iii) strong sensitivity to photon-ring coupling disorder, moderate sensitivity to energetic disorder, but weak sensitivity to intra-ring disorder, and (iv) robust recovery of performance by increasing g . These points form the core of our conclusions and are consistent across analytic baselines, loss-channel diagnostics, and full numerical results.

ACKNOWLEDGMENTS

OIRF is funded by the EPSRC via the Maths DTP 2021-22 University of Exeter (EP/W523859/1).

Appendix A: Operator Algebra

Each donor pigment is modeled as a 2-LS with ground $|g\rangle_j$ and excited $|e\rangle_j$ states. Writing Pauli ladder operators $\sigma_j^+ = |e\rangle_{jj}\langle g|$, $\sigma_j^- = |g\rangle_{jj}\langle e|$, and $\sigma_j^z = \frac{1}{2}(|e\rangle_{jj}\langle e| - |g\rangle_{jj}\langle g|)$, the *hard-core boson* language expresses the same algebra in terms of bosons that cannot doubly occupy a site. The Holstein-Primakoff (HP) map [35] gives an ex-

act operator identity for spin- S :

$$S_j^+ = b_j^\dagger \sqrt{2S - b_j^\dagger b_j}, \quad (\text{A1})$$

$$S_j^- = \sqrt{2S - b_j^\dagger b_j} b_j, \quad (\text{A2})$$

$$S_j^z = S - b_j^\dagger b_j, \quad (\text{A3})$$

where $[b_i, b_j^\dagger] = \delta_{ij}$ are *canonical* bosons. Identifying $\sigma_j^\pm = S_j^\pm$ and $\sigma_j^z = S_j^z$ with $S = \frac{1}{2}$ (2-LS) yields

$$\sigma_j^+ = b_j^\dagger \sqrt{1 - n_j}, \quad (\text{A4})$$

$$\sigma_j^- = \sqrt{1 - n_j} b_j, \quad (\text{A5})$$

$$\sigma_j^z = \frac{1}{2} - n_j, \quad (\text{A6})$$

$$n_j \equiv b_j^\dagger b_j, \quad (\text{A7})$$

where $n_j \in \{0, 1\}$. Equations (A4)-(A7) *enforce* the on-site exclusion ($n_j \in \{0, 1\}$) through the square roots, making the HP map *exact* for a 2-LS. In this sense, hard-core bosons are just canonical bosons with the nonlinearity $\sqrt{1 - n_j}$ that forbids double occupancy.

The projected ladder operators $e_j^\dagger \equiv \sigma_j^+$, $e_j \equiv \sigma_j^-$ satisfy $\{e_j, e_j^\dagger\} = 1$, $e_j^2 = (e_j^\dagger)^2 = 0$ (Pauli/hard-core at a site), while operators on different sites commute: $[e_i, e_j] = [e_i, e_j^\dagger] = 0$ for $i \neq j$. This is exactly what the HP representation implements when the square roots are kept.

For low excitation density (few excitations spread over many sites), one often *linearizes* HP by expanding $\sqrt{1 - n_j} \approx 1 - \frac{1}{2}n_j + \dots$ and retaining only the leading term:

$$\sigma_j^+ \approx b_j^\dagger, \quad \sigma_j^- \approx b_j, \quad \sigma_j^z \approx \frac{1}{2} - n_j. \quad (\text{A8})$$

This converts the problem into *free bosons*, which is *exact* whenever the Hilbert space is restricted so that no site is ever doubly occupied (e.g. the global single-excitation manifold). Beyond the single-excitation sector, the linearized form *must* be accompanied by either (i) explicit projectors $(1 - n_j)$, (ii) the full square roots, or (iii) an infinite on-site repulsion (hard-core limit of a Bose-Hubbard model) to prevent unphysical double occupancies.

Nearest-neighbor exciton transfer terms $J(\sigma_i^+ \sigma_j^- + \text{H.c.})$ map under exact HP to

$$J(b_i^\dagger \sqrt{1 - n_i} \sqrt{1 - n_j} b_j + \text{H.c.}). \quad (\text{A9})$$

At low density (or strictly within the single-excitation manifold), $\sqrt{1 - n_i} \sqrt{1 - n_j} \rightarrow 1$ and one recovers the familiar bosonic hopping $J(b_i^\dagger b_j + \text{H.c.})$ *exactly*. In multi-excitation sectors this number-dependent factor reduces the effective hopping into an already-occupied site and enforces saturation, which is essential for correctly capturing exciton-exciton blocking on a pigment.

With HP exact, population loss from an excited 2-LS site generated by $\mathcal{D}[\sigma_j^-]$ equals that generated by $\mathcal{D}[\sqrt{1-n_j}b_j]$. In linearized HP ($\sigma_j^- \approx b_j$), one must ensure the master equation never populates $n_j \geq 2$. This is automatic in the global single-excitation manifold and remains accurate at low densities, but for double-excitation simulations we recommend either keeping the $\sqrt{1-n_j}$ factors or adding an explicit hard-core constraint (e.g. projectors or a large on-site penalty) so that the Lindblad dynamics respect saturation.

a. When the HP/hard-core picture is exact vs. approximate.

- *Exact:* any 2-LS description (one exciton per pigment) provided the square roots are retained; all excitation densities; any Hamiltonian/Lindbladian built from σ_j^\pm, σ_j^z .
- *Exact by restriction:* global single-excitation manifold (at most one excitation in the entire ring): the linearized HP is indistinguishable from exact dynamics because double occupancy cannot occur.
- *Approximate:* linearized HP in multi-excitation sectors without constraints; accuracy improves as the density per site $\langle n_j \rangle \ll 1$.

b. Generalizations. If a pigment admits up to 2S local excitations (e.g. a three-level ladder), use HP with $S > 1/2$: $S_j^\pm = b_j^\dagger \sqrt{2S-n_j}$, $S_j^z = S - n_j$. The hard-core case is $S = \frac{1}{2}$. For strictly one-dimensional rings one may alternatively enforce exclusion via a Jordan–Wigner map to fermions; however, for our purposes HP with hard-core (Pauli) operators is both local and directly aligned with the two-level chromophore model.

Appendix B: Explicit mapping to a V system

This section makes explicit the mapping from the LH1–RC ring model to the minimal three-level “V system” (two upper states feeding one acceptor/sink) introduced earlier, and shows how it captures coherent trapping, ENAQT, and disorder-activated losses. We present two equivalent viewpoints: a concrete *site-dimer truncation* and a *collective (bright/dark) coarse-graining*. Throughout we use the Lindblad-rate convention

$$\mathcal{L}[L]\rho = \Gamma(2L\rho L^\dagger - \{L^\dagger L, \rho\}), \quad (\text{B1})$$

so populations decay as 2Γ , and we also write the shorthand dissipator

$$\mathcal{D}[X]\rho \equiv 2X\rho X^\dagger - \{X^\dagger X, \rho\}. \quad (\text{B2})$$

1. A. Site-dimer truncation \rightarrow V system (most concrete)

Pick two representative donors on the ring (sites A and B) and the acceptor C. Restrict the single-excitation

Hilbert space to

$$\{|A\rangle, |B\rangle, |C\rangle\}. \quad (\text{B3})$$

In a rotating frame, the Hamiltonian and dissipators read

$$H_V = \omega_d(|A\rangle\langle A| + |B\rangle\langle B|) + \omega_a|C\rangle\langle C| - J(|A\rangle\langle B| + |B\rangle\langle A|) - \xi(|A\rangle\langle C| + |B\rangle\langle C| + \text{H.c.}), \quad (\text{B4})$$

$$\dot{\rho}|_{\text{loss}} = \kappa \sum_{s=A,B} \mathcal{D}[|G\rangle\langle s|]\rho + \Gamma \mathcal{D}[|\text{sink}\rangle\langle C|]\rho, \quad (\text{B5})$$

$$\dot{\rho}|_{\text{deph}} = \gamma \sum_{s=A,B} \mathcal{D}[|s\rangle\langle s|]\rho, \quad (\text{B6})$$

with $\Delta = \omega_a - \omega_d$ the local donor–acceptor detuning. A narrowband photon can be added (equal-phase drive on A and B).

a. Bright/dark basis inside the V system. Define

$$|+\rangle = \frac{|A\rangle + |B\rangle}{\sqrt{2}}, \quad |-\rangle = \frac{|A\rangle - |B\rangle}{\sqrt{2}}. \quad (\text{B7})$$

Then C couples only to $|+\rangle$ with strength $\sqrt{2}\xi$, while $|-\rangle$ is *dark* (no matrix element to C). The A–B tunneling J sets the internal splitting $E_\pm = \omega_d \mp J$. A symmetric optical drive (equal phase on A and B) pumps $|+\rangle$ exclusively. Thus the V system exhibits coherent trapping in $|-\rangle$ at $\gamma = 0$, and ENAQT when moderate dephasing γ mixes $|-\rangle \leftrightarrow |+\rangle$.

b. Parameter mapping. J is the donor–donor coupling on that bond (ring g locally); ξ is the donor–acceptor coupling; κ, Γ, γ are the donor loss, acceptor extraction, and donor dephasing rates (populations decay as $2\kappa, 2\Gamma$ under (B1)).

2. B. Collective (bright/dark) coarse-graining \rightarrow effective V system

For the ordered ring, define the *bright* collective state

$$|B_0\rangle = \frac{1}{\sqrt{N}} \sum_{j=1}^N |j\rangle, \quad \omega_0 = \omega_d + 2g, \quad (\text{B8})$$

and choose any orthonormal *dark* superposition $|D\rangle$ from the $(N-1)$ -dimensional dark subspace (e.g., the lowest- $|k|$ eigenmode) with energy ω_D . Keep the acceptor $|C\rangle$. Retaining these three states yields an effective V geometry:

$$H_{\text{eff}} = \omega_0|B_0\rangle\langle B_0| + \omega_D|D\rangle\langle D| + \omega_a|C\rangle\langle C| - \xi_{\text{eff}}|B_0\rangle\langle C| + \text{H.c.} + V_{\text{mix}}(|B_0\rangle\langle D| + \text{H.c.}), \quad (\text{B9})$$

with $\xi_{\text{eff}} = \sqrt{N}\xi$. In the perfectly symmetric, noise-free limit $V_{\text{mix}} = 0$. Static disorder (e.g., photon–ring coupling disorder J_j) and pure dephasing generate an effective bright–dark mixing V_{mix} (coherent or Liouvillian), opening dissipation channels through dark states.

a. Interpretation. The collective mapping is the right language to explain whole-ring numerics: why photon–ring coupling disorder reduces efficiency (it increases effective mixing into dark modes), and why increasing intra-ring coupling g moves ω_D away from the dressed bright–acceptor energy, mitigating loss near the operating detuning.

3. C. Drives and conventions (consistent with the main text)

- **Optical drive.** In the site–dimer mapping, a symmetric narrowband drive pumps $|+\rangle$; in the collective mapping it pumps $|B_0\rangle$.
- **Rates.** With $\mathcal{L}[L]$ as in (B1), populations on A,B decay at 2κ , on C at 2Γ ; coherences acquire the usual half-sum of the connected decay rates.
- **Detunings.** Local: $\delta = \omega_p - \omega_d$, $\Delta = \omega_a - \omega_d$. Dimensionless: $\tilde{\delta} = (\omega_p - \omega_a)/\xi$.

4. D. When the two mappings make the same predictions

- **Ordered, symmetric, on resonance.** Both reduce to a bright-only pathway; the dark channel is decoupled \Rightarrow tall, narrow efficiency peak.
- **Moderate dephasing.** Both exhibit ENAQT off resonance by mixing the dark channel back into the bright pathway; on resonance, dephasing narrows/lowers the peak.
- **Photon–ring coupling and energetic disorder.** Both represent it as extra coupling into the dark channel (drive imbalance in the dimer picture, nonzero V_{mix} in the collective picture), yielding loss bands where ω_D crosses the dressed bright–acceptor eigenenergy.
- **Increasing g .** Both shift dark energies away from the operating point, mitigating disorder-activated loss and restoring near-peak performance.

5. E. Quick recipe for analysis and numerics

a. V system from a site pair (A,B,C). Set $J = g$, $\xi, \kappa, \Gamma, \gamma$ as in the ring. Drive A and B with equal phase; work in the $|\pm\rangle, C$ basis. This 3×3 Liouvillian is *exactly solvable* in the single-excitation sector and provides a clean benchmark for trapping vs ENAQT.

b. V system from collective modes (B_0, D, C). Use $\xi_{\text{eff}} = \sqrt{N}\xi$, $\omega_0 = \omega_d + 2g$, and choose ω_D from the ring spectrum. Model disorder/dephasing as a small bright–dark mixing V_{mix} (coherent and/or dissipative). Use this to interpret full-ring numerics and to formulate design rules (e.g., choose g so $\min_k |\omega_k - \epsilon_{2\delta_{op}}|$ exceeds the broadened linewidth).

Either mapping supplies a one-to-one dictionary from LH1–RC parameters to a V -system parameters, explains coherent trapping, ENAQT, and disorder-activated losses, and yields compact, exactly solvable baselines that validate and interpret the full simulations.

Appendix C: Coherent Evolution of Collective Mode Operators

The closed quantum system (without coupling to the environment), has time evolution governed by the Von-Neumann equation through a Hamiltonian H , as follows

$$\frac{d\rho}{dt} = \dot{\rho} = -i[H, \rho]. \quad (\text{C1})$$

We consider the time evolution of operator averages using Eq. (17). As we are interested in the time evolution of the populations, we first consider $\langle a^\dagger a \rangle$, the average number of excitations on the acceptor, which, because the acceptor is a 2-LS, is equivalent to the probability that the acceptor is excited. By substituting $\langle a^\dagger a \rangle$ in Eq. (17), we obtain

$$\frac{d\langle a^\dagger a \rangle}{dt} = -i \text{Tr}[a^\dagger a (H\rho - \rho H)]. \quad (\text{C2})$$

We obtain a set of coupled equations for the time evolution of the population expectation values as follows

$$\frac{d\langle a^\dagger a \rangle}{dt} = i\sqrt{N}\xi(\langle \tilde{\mathbf{e}}_0^\dagger a \rangle - \langle a^\dagger \tilde{\mathbf{e}}_0 \rangle), \quad (\text{C3a})$$

$$\frac{d\langle c_p^\dagger c_p \rangle}{dt} = i\sqrt{N}J(\langle \tilde{\mathbf{e}}_0^\dagger c_p \rangle - \langle c_p^\dagger \tilde{\mathbf{e}}_0 \rangle), \quad (\text{C3b})$$

$$\begin{aligned} \frac{d\langle \tilde{\mathbf{e}}_0^\dagger \tilde{\mathbf{e}}_0 \rangle}{dt} &= i\sqrt{N}\xi(\langle a^\dagger \tilde{\mathbf{e}}_0 \rangle - \langle \tilde{\mathbf{e}}_0^\dagger a \rangle) \\ &\quad + i\sqrt{N}J(\langle c_p^\dagger \tilde{\mathbf{e}}_0 \rangle - \langle \tilde{\mathbf{e}}_0^\dagger c_p \rangle), \end{aligned} \quad (\text{C3c})$$

$$\begin{aligned} \frac{d\langle \tilde{\mathbf{e}}_0^\dagger a \rangle}{dt} &= -i(\Delta - 2g)\langle \tilde{\mathbf{e}}_0^\dagger a \rangle + i\sqrt{N}\xi(\langle a^\dagger a \rangle - \langle \tilde{\mathbf{e}}_0^\dagger \tilde{\mathbf{e}}_0 \rangle) \\ &\quad + i\sqrt{N}J\langle c_p^\dagger a \rangle, \end{aligned} \quad (\text{C3d})$$

$$\begin{aligned} \frac{d\langle \tilde{\mathbf{e}}_0^\dagger c_p \rangle}{dt} &= -i(\delta - 2g)\langle \tilde{\mathbf{e}}_0^\dagger c_p \rangle + i\sqrt{N}J(\langle c_p^\dagger c_p \rangle - \langle \tilde{\mathbf{e}}_0^\dagger \tilde{\mathbf{e}}_0 \rangle) \\ &\quad + i\sqrt{N}\xi\langle a^\dagger c_p \rangle, \end{aligned} \quad (\text{C3e})$$

$$\frac{d\langle a^\dagger c_p \rangle}{dt} = i(\Delta - \delta)\langle a^\dagger c_p \rangle + i\sqrt{N}\xi\langle \tilde{\mathbf{e}}_0^\dagger c_p \rangle - i\sqrt{N}J\langle a^\dagger \tilde{\mathbf{e}}_0 \rangle, \quad (\text{C3f})$$

where $\delta = \omega_p - \omega_d$ and $\Delta = \omega_a - \omega_d$. We have used the following anti-commutation relations

$$\{a, a^\dagger\} = 1, \quad \{e_i, e_j^\dagger\} = \delta_{ij}, \quad \{c_p, c_p^\dagger\} = 1. \quad (\text{C4})$$

Also, we note that the $k \neq 0$ donor-ring modes do not appear in the set of equations.

Appendix D: Coherent and Incoherent Evolution of Collective Mode Operators

Introducing the Lindblad terms in Eq. (9), the equation for an arbitrary operator expectation value $\langle O(t) \rangle$

$$\begin{aligned} \frac{d\langle O(t) \rangle}{dt} = & -i \text{Tr}[O[H, \rho]] + \text{Tr}[O\mathcal{L}_D(\rho)] \\ & + \text{Tr}[O\mathcal{L}_A(\rho)] + \text{Tr}[O\mathcal{L}_P(\rho)]. \end{aligned} \quad (\text{D1})$$

As c_p and c_p^\dagger do not appear in the superoperators, \mathcal{L}_D , \mathcal{L}_A and \mathcal{L}_P , the equation of motion for $\langle c_p^\dagger c_p \rangle$ is the same as Eq. (C3b). For $\langle a^\dagger a \rangle$, we find

$$\text{Tr}[a^\dagger a \mathcal{L}_A] = -2\Gamma\langle a^\dagger a \rangle, \quad \text{Tr}[a^\dagger a \mathcal{L}_D] = \text{Tr}[a^\dagger a \mathcal{L}_P] = 0, \quad (\text{D2})$$

which gives the full equation of motion as

$$\frac{d\langle a^\dagger a \rangle}{dt} = -2\Gamma\langle a^\dagger a \rangle + i\sqrt{N}\xi(\langle \tilde{\mathbf{e}}_0^\dagger a \rangle - \langle a^\dagger \tilde{\mathbf{e}}_0 \rangle). \quad (\text{D3})$$

For $\langle a^\dagger c_p \rangle$, we find the traces

$$\begin{aligned} \text{Tr}[a^\dagger c_p \mathcal{L}_A] &= -\Gamma\langle a^\dagger c_p \rangle, \\ \text{Tr}[a^\dagger c_p \mathcal{L}_D] &= \text{Tr}[a^\dagger c_p \mathcal{L}_P] = 0, \end{aligned} \quad (\text{D4})$$

which gives the equation of motion for $\langle a^\dagger c_p \rangle$ and, by taking Hermitian conjugate, $\langle c_p^\dagger a \rangle$, as

$$\begin{aligned} \frac{d\langle a^\dagger c_p \rangle}{dt} &= (i(\Delta - \delta) - \Gamma)\langle a^\dagger c_p \rangle \\ &+ i\sqrt{N}\xi\langle \tilde{\mathbf{e}}_0^\dagger c_p \rangle - i\sqrt{N}J\langle a^\dagger \tilde{\mathbf{e}}_0 \rangle, \end{aligned} \quad (\text{D5})$$

$$\begin{aligned} \frac{d\langle c_p^\dagger a \rangle}{dt} &= (i(\delta - \Delta) - \Gamma)\langle c_p^\dagger a \rangle \\ &+ i\sqrt{N}J\langle \tilde{\mathbf{e}}_0^\dagger a \rangle - i\sqrt{N}\xi\langle c_p^\dagger \tilde{\mathbf{e}}_0 \rangle. \end{aligned} \quad (\text{D6})$$

To calculate the trace terms for the momentum space operators, we need to first calculate them for the real space operators, as follows

$$\text{Tr}[a^\dagger e_j \mathcal{L}_A] = -\Gamma\langle a^\dagger e_j \rangle, \quad (\text{D7a})$$

$$\text{Tr}[a^\dagger e_j \mathcal{L}_D] = -\kappa\langle a^\dagger e_j \rangle, \quad (\text{D7b})$$

$$\text{Tr}[a^\dagger e_j \mathcal{L}_P] = -\gamma\langle a^\dagger e_j \rangle, \quad (\text{D7c})$$

These are then used to calculate trace terms for $a^\dagger \tilde{\mathbf{e}}_k$ as follows

$$\begin{aligned} \text{Tr}[a^\dagger \tilde{\mathbf{e}}_0 \mathcal{L}_A] &= \frac{1}{\sqrt{N}} \sum_{j=1}^N \text{Tr}[a^\dagger e_j \mathcal{L}_D] \\ &= -\Gamma \frac{1}{\sqrt{N}} \sum_{j=1}^N \langle a^\dagger e_j \rangle = -\Gamma\langle a^\dagger \tilde{\mathbf{e}}_0 \rangle, \end{aligned} \quad (\text{D8a})$$

$$\begin{aligned} \text{Tr}[a^\dagger \tilde{\mathbf{e}}_0 \mathcal{L}_D] &= \frac{1}{\sqrt{N}} \sum_{j=1}^N \text{Tr}[a^\dagger e_j \mathcal{L}_D] \\ &= -\kappa \frac{1}{\sqrt{N}} \sum_{j=1}^N \langle a^\dagger e_j \rangle = -\kappa\langle a^\dagger \tilde{\mathbf{e}}_0 \rangle, \end{aligned} \quad (\text{D8b})$$

$$\begin{aligned} \text{Tr}[a^\dagger \tilde{\mathbf{e}}_0 \mathcal{L}_P] &= \frac{1}{\sqrt{N}} \sum_{j=1}^N \text{Tr}[a^\dagger e_j \mathcal{L}_D] \\ &= -\gamma \frac{1}{\sqrt{N}} \sum_{j=1}^N \langle a^\dagger e_j \rangle = -\gamma\langle a^\dagger \tilde{\mathbf{e}}_0 \rangle. \end{aligned} \quad (\text{D8c})$$

Which combined with the Hamiltonian term in Eq. (C3), gives

$$\begin{aligned} \frac{d\langle a^\dagger \tilde{\mathbf{e}}_0 \rangle}{dt} &= (i(\Delta - 2g) - (\gamma + \Gamma + \kappa))\langle a^\dagger \tilde{\mathbf{e}}_0 \rangle \\ &+ i\sqrt{N}\xi(\langle \tilde{\mathbf{e}}_0^\dagger \tilde{\mathbf{e}}_0 \rangle - \langle a^\dagger a \rangle) - i\sqrt{N}J\langle a^\dagger c_p \rangle, \end{aligned} \quad (\text{D9})$$

and by taking the Hermitian conjugate, we obtain the equation for $\langle \tilde{\mathbf{e}}_0^\dagger a \rangle$ as

$$\begin{aligned} \frac{d\langle \tilde{\mathbf{e}}_0^\dagger a \rangle}{dt} &= (-i(\Delta - 2g) - (\gamma + \Gamma + \kappa))\langle \tilde{\mathbf{e}}_0^\dagger a \rangle \\ &+ i\sqrt{N}\xi(\langle a^\dagger a \rangle - \langle \tilde{\mathbf{e}}_0^\dagger \tilde{\mathbf{e}}_0 \rangle) + i\sqrt{N}J\langle c_p^\dagger a \rangle. \end{aligned} \quad (\text{D10})$$

Noting that $\text{Tr}[\tilde{\mathbf{e}}_0^\dagger c_p \mathcal{L}_A(\rho)] = 0$, the same argument can be applied to find the equations for $\langle \tilde{\mathbf{e}}_0^\dagger c_p \rangle$ and $\langle c_p^\dagger \tilde{\mathbf{e}}_0 \rangle$ as

$$\begin{aligned} \frac{d\langle \tilde{\mathbf{e}}_0^\dagger c_p \rangle}{dt} &= (-i(\delta - 2g) - (\gamma + \kappa))\langle \tilde{\mathbf{e}}_0^\dagger c_p \rangle \\ &+ i\sqrt{N}J(\langle c_p^\dagger c_p \rangle - \langle \tilde{\mathbf{e}}_0^\dagger \tilde{\mathbf{e}}_0 \rangle) + i\sqrt{N}\xi\langle a^\dagger c_p \rangle, \end{aligned} \quad (\text{D11})$$

$$\begin{aligned} \frac{d\langle c_p^\dagger \tilde{\mathbf{e}}_0 \rangle}{dt} &= (i(\delta - 2g) - (\gamma + \kappa))\langle c_p^\dagger \tilde{\mathbf{e}}_0 \rangle \\ &+ i\sqrt{N}J(\langle \tilde{\mathbf{e}}_0^\dagger \tilde{\mathbf{e}}_0 \rangle - \langle c_p^\dagger c_p \rangle) - i\sqrt{N}\xi\langle c_p^\dagger a \rangle. \end{aligned} \quad (\text{D12})$$

Finally, the trace terms involving $e_j^\dagger e_{j'}$ are

$$\text{Tr}[e_j^\dagger e_{j'} \mathcal{L}_A] = 0, \quad (\text{D13a})$$

$$\text{Tr}[e_j^\dagger e_{j'} \mathcal{L}_D] = -2\kappa \langle e_j^\dagger e_{j'} \rangle, \quad (\text{D13b})$$

$$\text{Tr}[e_j^\dagger e_{j'} \mathcal{L}_P] = -2\gamma \langle e_j^\dagger e_{j'} \rangle (1 - \delta_{jj'}). \quad (\text{D13c})$$

Notably, the dephasing term in Eq. (D13c) does not effect the populations, $\langle e_j^\dagger e_j \rangle$, but only the coherence terms, $\langle e_j^\dagger e_{j'} \rangle$. If we now consider the k -space operators in Eq. (11), we can calculate the trace terms

$$\begin{aligned} \text{Tr}[\tilde{\mathbf{e}}_k^\dagger \tilde{\mathbf{e}}_k \mathcal{L}_D] &= \frac{1}{N} \sum_{j,j'} e^{ik(j'-j)} \text{Tr}[e_j^\dagger e_{j'} \mathcal{L}_D] \\ &= -\frac{2\kappa}{N} \sum_{j,j'} e^{ik(j'-j)} \langle e_j^\dagger e_{j'} \rangle = -2\kappa \langle \tilde{\mathbf{e}}_k^\dagger \tilde{\mathbf{e}}_k \rangle, \end{aligned} \quad (\text{D14a})$$

$$\begin{aligned} \text{Tr}[\tilde{\mathbf{e}}_k^\dagger \tilde{\mathbf{e}}_k \mathcal{L}_P] &= \frac{1}{N} \sum_{j,j'} e^{ik(j'-j)} \text{Tr}[e_j^\dagger e_{j'} \mathcal{L}_P] \\ &= -\frac{2\gamma}{N} \sum_{j,j'} e^{ik(j'-j)} \langle e_j^\dagger e_{j'} \rangle (1 - \delta_{jj'}) \\ &= -\frac{2\gamma}{N} \left(\sum_{j,j'} e^{ik(j'-j)} \langle e_j^\dagger e_{j'} \rangle - \sum_j \langle e_j^\dagger e_j \rangle \right) \\ &= -2\gamma \left(\langle \tilde{\mathbf{e}}_k^\dagger \tilde{\mathbf{e}}_k \rangle - \frac{1}{N} \sum_{k'} \langle \tilde{\mathbf{e}}_{k'}^\dagger \tilde{\mathbf{e}}_{k'} \rangle \right), \end{aligned} \quad (\text{D14b})$$

where we have used

$$\sum_{j=1}^N \langle e_j^\dagger e_j \rangle = \sum_k \langle \tilde{\mathbf{e}}_k^\dagger \tilde{\mathbf{e}}_k \rangle. \quad (\text{D15})$$

For $k = 0$, these equations become

$$\text{Tr}[\tilde{\mathbf{e}}_0^\dagger \tilde{\mathbf{e}}_0 \mathcal{L}_D] = -2\kappa \langle \tilde{\mathbf{e}}_0^\dagger \tilde{\mathbf{e}}_0 \rangle, \quad (\text{D16a})$$

$$\text{Tr}[\tilde{\mathbf{e}}_0^\dagger \tilde{\mathbf{e}}_0 \mathcal{L}_P] = -2\gamma \left(\left(1 - \frac{1}{N}\right) \langle \tilde{\mathbf{e}}_0^\dagger \tilde{\mathbf{e}}_0 \rangle - \frac{1}{N} \langle \tilde{\mathbf{e}}_k^\dagger \tilde{\mathbf{e}}_k \rangle_L \right), \quad (\text{D16b})$$

where we have introduced $\langle \tilde{\mathbf{e}}_k^\dagger \tilde{\mathbf{e}}_k \rangle_L$, the sum of the expectations of the $k \neq 0$ populations operators,

$$\langle \tilde{\mathbf{e}}_k^\dagger \tilde{\mathbf{e}}_k \rangle_L = \sum_{k \neq 0} \langle \tilde{\mathbf{e}}_k^\dagger \tilde{\mathbf{e}}_k \rangle. \quad (\text{D17})$$

This gives the equation of motion for $\langle \tilde{\mathbf{e}}_0^\dagger \tilde{\mathbf{e}}_0 \rangle$, as

$$\begin{aligned} \frac{d\langle \tilde{\mathbf{e}}_0^\dagger \tilde{\mathbf{e}}_0 \rangle}{dt} &= -2 \left(\kappa + \gamma \left(1 - \frac{1}{N}\right) \right) \langle \tilde{\mathbf{e}}_0^\dagger \tilde{\mathbf{e}}_0 \rangle + \frac{2\gamma}{N} \langle \tilde{\mathbf{e}}_k^\dagger \tilde{\mathbf{e}}_k \rangle_L \\ &\quad + i\sqrt{N}\xi(\langle a^\dagger \tilde{\mathbf{e}}_0 \rangle - \langle \tilde{\mathbf{e}}_0^\dagger a \rangle) + i\sqrt{N}J(\langle c_p^\dagger \tilde{\mathbf{e}}_0 \rangle - \langle \tilde{\mathbf{e}}_0^\dagger c_p \rangle), \end{aligned} \quad (\text{D18})$$

In Eq. (D18) we need to determine the equation of motion for $\langle \tilde{\mathbf{e}}_k^\dagger \tilde{\mathbf{e}}_k \rangle_L$, since we already have the equations of motion for the other operators in Eq. (C3). Since only the $k = 0$ mode couples to the acceptor, we observe that for $k \neq 0$,

$$\text{Tr}[-i\tilde{\mathbf{e}}_k^\dagger \tilde{\mathbf{e}}_k [H, \rho]] = 0. \quad (\text{D19})$$

From Eq. (D14) we obtain the following

$$\sum_{k \neq 0} \text{Tr}[\tilde{\mathbf{e}}_k^\dagger \tilde{\mathbf{e}}_k \mathcal{L}_D] = -2\kappa \sum_{k \neq 0} \langle \tilde{\mathbf{e}}_k^\dagger \tilde{\mathbf{e}}_k \rangle = -2\kappa \langle \tilde{\mathbf{e}}_k^\dagger \tilde{\mathbf{e}}_k \rangle_L, \quad (\text{D20a})$$

$$\begin{aligned} \sum_{k \neq 0} \text{Tr}[\tilde{\mathbf{e}}_k^\dagger \tilde{\mathbf{e}}_k \mathcal{L}_P] &= 2\gamma \left(\frac{N-1}{N} \langle \tilde{\mathbf{e}}_0^\dagger \tilde{\mathbf{e}}_0 \rangle - \frac{1}{N} \sum_{k \neq 0} \langle \tilde{\mathbf{e}}_k^\dagger \tilde{\mathbf{e}}_k \rangle \right) \\ &= 2\gamma \left(\frac{N-1}{N} \langle \tilde{\mathbf{e}}_0^\dagger \tilde{\mathbf{e}}_0 \rangle - \frac{1}{N} \langle \tilde{\mathbf{e}}_k^\dagger \tilde{\mathbf{e}}_k \rangle_L \right), \end{aligned} \quad (\text{D20b})$$

which combine to give

$$\frac{d\langle \tilde{\mathbf{e}}_k^\dagger \tilde{\mathbf{e}}_k \rangle_L}{dt} = 2 \left(-\kappa - \frac{\gamma}{N} \right) \langle \tilde{\mathbf{e}}_k^\dagger \tilde{\mathbf{e}}_k \rangle_L + 2\gamma \left(1 - \frac{1}{N} \right) \langle \tilde{\mathbf{e}}_0^\dagger \tilde{\mathbf{e}}_0 \rangle. \quad (\text{D21})$$

In matrix form, these equations can be written as

$$\frac{d\mathbf{P}(t)}{dt} = \mathbf{M}\mathbf{P}(t), \quad (\text{D22})$$

where

$$\mathbf{P}(t) = \left(\langle c_p^\dagger c_p(t) \rangle \quad \langle a^\dagger a(t) \rangle \quad \langle \tilde{\mathbf{e}}_0^\dagger \tilde{\mathbf{e}}_0(t) \rangle \quad \langle \tilde{\mathbf{e}}_0^\dagger c_p(t) \rangle \quad \langle c_p^\dagger \tilde{\mathbf{e}}_0(t) \rangle \quad \langle a^\dagger c_p(t) \rangle \quad \langle c_p^\dagger a(t) \rangle \quad \langle \tilde{\mathbf{e}}_0^\dagger a(t) \rangle \quad \langle a^\dagger \tilde{\mathbf{e}}_0(t) \rangle \quad \langle \tilde{\mathbf{e}}_k^\dagger \tilde{\mathbf{e}}_k(t) \rangle_L \right)^T, \quad (\text{D23a})$$

$$\mathbf{M} = \begin{pmatrix} 0 & 0 & 0 & iJ\sqrt{N} & -iJ\sqrt{N} & 0 & 0 & 0 & 0 & 0 \\ 0 & -2\Gamma & 0 & 0 & 0 & 0 & 0 & -i\sqrt{N}\xi & i\sqrt{N}\xi & 0 \\ 0 & 0 & -2(\kappa + \gamma(1 - \frac{1}{N})) & -iJ\sqrt{N} & iJ\sqrt{N} & 0 & 0 & i\sqrt{N}\xi & -i\sqrt{N}\xi & \frac{2\gamma}{N} \\ iJ\sqrt{N} & 0 & -iJ\sqrt{N} & -i\delta_c - \gamma - \kappa & 0 & i\sqrt{N}\xi & 0 & 0 & 0 & 0 \\ -iJ\sqrt{N} & 0 & iJ\sqrt{N} & 0 & i\delta_c - \gamma - \kappa & 0 & -i\sqrt{N}\xi & 0 & 0 & 0 \\ 0 & 0 & 0 & i\sqrt{N}\xi & 0 & i(\Delta - \delta) - \Gamma & 0 & -iJ\sqrt{N} & 0 & 0 \\ 0 & 0 & 0 & 0 & -i\sqrt{N}\xi & 0 & i(\delta - \Delta) - \Gamma & 0 & iJ\sqrt{N} & 0 \\ 0 & -i\sqrt{N}\xi & i\sqrt{N}\xi & 0 & 0 & -iJ\sqrt{N} & 0 & i\Delta_c - \gamma - \kappa - \Gamma & 0 & 0 \\ 0 & i\sqrt{N}\xi & -i\sqrt{N}\xi & 0 & 0 & 0 & iJ\sqrt{N} & 0 & -i\Delta_c - \gamma - \kappa - \Gamma & 0 \\ 0 & 0 & \frac{2\gamma(N-1)}{N} & 0 & 0 & 0 & 0 & 0 & 0 & -\frac{2\gamma}{N} - 2\kappa \end{pmatrix}, \quad (\text{D23b})$$

where $\delta_c = \delta - 2g$ and $\Delta_c = \Delta - 2g$. The matrix \mathbf{M} can be used to calculate the losses L_k ($k \neq 0$) in Eq. (25), which are found as

$$\begin{aligned} L_k = & \gamma\kappa \left(\Delta_c^4 \mu\Gamma + \delta_c^2 (\Delta_c^2 \mu\Gamma + \nu^2 (\mu\Gamma + N\xi^2)) + \Delta_c^2 (\mu\Gamma (\gamma^2 + 2\kappa(\gamma + \Gamma) + 2\gamma\Gamma - 2J^2N + \kappa^2 + 2\Gamma^2) + N\nu^2\xi^2) \right. \\ & \left. - 2\Delta_c\delta_c\mu\Gamma (\Delta_c^2 - J^2N + \nu^2) - 2\Delta_c\delta_cN\nu^2\xi^2 + \Gamma (J^2N + \nu\Gamma) (\mu (J^2N + \nu\Gamma) + N\nu\xi^2) \right) / \\ & N \left(\delta_c^2 \mu (\kappa\mu\Gamma (\Delta_c^2 + \nu^2) + \nu\xi^2(\gamma\Gamma + \kappa N\nu)) - 2\delta_c\Delta_c\mu (\kappa\mu\Gamma (\Delta_c^2 - J^2N + \nu^2) + \nu\xi^2(\gamma\Gamma + \kappa N\nu)) + \Delta_c^4 \kappa\mu^2\Gamma \right. \\ & + \Delta_c^2 \mu (\kappa\mu\Gamma (\gamma^2 + 2\kappa(\gamma + \Gamma) + 2\gamma\Gamma - 2J^2N + \kappa^2 + 2\Gamma^2) + \xi^2 (\kappa N (\gamma^2 + 2\kappa(\gamma + \Gamma) + 2\gamma\Gamma + \kappa^2 + 2\Gamma^2) + \gamma\nu\Gamma)) \\ & \left. + \Gamma (\mu (J^2N + \nu\Gamma) + N\nu\xi^2) (\xi^2(\gamma\Gamma + \kappa N\nu) + \kappa\mu (J^2N + \nu\Gamma)) \right), \end{aligned} \quad (\text{D24})$$

where $\mu = \kappa + \gamma$ and $\nu = \kappa + \gamma + \Gamma$.

Appendix E: Transfer Efficiency

The Laplace transformation $F(s)$ of an arbitrary function $f(t)$, is defined as

$$F(s) = \mathbf{L}[f(t)]_s = \int_0^\infty e^{-st} f(t) dt, \quad (\text{E1})$$

where s is a complex parameter. The Laplace transform of the time derivative of a function is

$$\mathbf{L} \left[\frac{df(t)}{dt} \right]_s = sF(s) - f(0). \quad (\text{E2})$$

For a system of equations that can be written in the following form

$$\frac{d\mathbf{P}(t)}{dt} = \mathbf{M}\mathbf{P}(t), \quad (\text{E3})$$

where $\mathbf{P}(t)$ is a column vector containing each operator expectation value, and \mathbf{M} is a square matrix of dimension m , the Laplace transform of Eq. (E3) is given as

$$s\tilde{\mathbf{P}}(s) - \mathbf{P}(0) = \mathbf{M}\tilde{\mathbf{P}}(s), \quad (\text{E4})$$

where $\tilde{\mathbf{P}}(s)$ is the Laplace transform of $\mathbf{P}(t)$. This can be rearranged as

$$\mathbf{A}(s)\tilde{\mathbf{P}}(s) = -\mathbf{P}(0), \quad (\text{E5})$$

where $\mathbf{A}(s) = \mathbf{M} - s\mathbf{I}$ and \mathbf{I} is the identity matrix. Pre-multiplying both sides of Eq. (E5) by $\mathbf{A}^{-1}(s)$, we obtain

$$\tilde{\mathbf{P}}(s) = -\frac{1}{\det[\mathbf{A}(s)]} \mathbf{C}^T \mathbf{P}(0), \quad (\text{E6})$$

where

$$\mathbf{A}^{-1}(s) = \frac{\mathbf{C}^T}{\det[\mathbf{A}(s)]}, \quad (\text{E7})$$

and \mathbf{C}^T is the transpose of the co-factor matrix of $\mathbf{A}(s)$. The determinant of $\mathbf{A}(s)$ is the determinant of $(\mathbf{M} - s\mathbf{I})$, which is given as

$$\det[\mathbf{A}(s)] = \prod_{j=1}^m (\epsilon_M^{(j)} - s), \quad (\text{E8})$$

where $\epsilon_M^{(j)}$ ($j = \{1, \dots, m\}$) are the eigenvalues of matrix \mathbf{M} .

The initial condition is $\langle c_p^\dagger c_p(0) \rangle = 1$. For the LH1-RC system with a single photon, we consider the vector $\mathbf{P}(t)$ and matrix \mathbf{M} , as defined in Eq. (D23a) and (D23b), respectively. Note that the first and second elements of $\mathbf{P}(t)$, i.e. $p_1(t)$ and $p_2(t)$, are $\langle c_p^\dagger c_p(t) \rangle$ and $\langle a^\dagger a(t) \rangle$, respectively. $\langle a^\dagger a(t) \rangle$ can be found via an inverse transformation on the second element of $\tilde{\mathbf{P}}(s)$ in Eq. (E6), which is

$$\langle a^\dagger a(s) \rangle = -\frac{1}{\det[\mathbf{A}(s)]} c_{12}^T. \quad (\text{E9})$$

where c_{12}^T is the $(1, 2)^{th}$ element of \mathbf{C}^T , which is calculated as

$$c_{12}^T = -\det[\mathbf{A}_{2,1}^M(s)], \quad (\text{E10})$$

where $\mathbf{A}_{2,1}^M(s)$ is the $(2, 1)^{th}$ sub-matrix of $\mathbf{A}(s)$. It should be noted that the sub-matrix, $\mathbf{A}_{i,j}^M$, is constructed by

eliminating the i^{th} row and j^{th} column from matrix \mathbf{A} . The determinant of $\mathbf{A}_{2,1}^M(s)$ gives the following characteristic polynomial

$$\det[\mathbf{A}_{2,1}^M] = \sum_{j=0}^9 a_j s^j, \quad (\text{E11})$$

where a_j is the coefficient of s^j . We note that $\mathbf{A}_{2,1}^M(s)$ is an 9×9 matrix so its determinant is a polynomial of degree 9. Substituting Eq. (E8) and (E11) into Eq. (E9) gives

$$\langle a^\dagger a(s) \rangle = \frac{\sum_{j=0}^9 a_j s^j}{\prod_{i=1}^{10} (\epsilon_M^{(i)} - s)}. \quad (\text{E12})$$

Applying an inverse Laplace transformation to Eq. (E12) gives $\langle a^\dagger a(t) \rangle$ as (see Appendix F)

$$\langle a^\dagger a(t) \rangle = \sum_{k=1}^{10} \left(\frac{e^{\epsilon_M^{(k)} t}}{\prod_{i \neq k} (\epsilon_M^{(k)} - \epsilon_M^{(i)})} \sum_{j=0}^9 a_j (\epsilon_M^{(k)})^j \right). \quad (\text{E13})$$

We can substitute the r.h.s. of Eq. (E13) into the integral in Eq. (20) and thereby obtain the transfer efficiency η . Since the polynomial in Eq. (E11) has order less than $N = 10$, the $j \neq 0$ terms cancel, and we find the efficiency, η , as

$$\eta = 2\Gamma \frac{a_0}{\prod_{j=1}^{10} \epsilon_M^{(j)}}. \quad (\text{E14})$$

We note that the denominator is the determinant of matrix \mathbf{M} , and the numerator is the determinant of the $(2, 1)^{th}$ sub-matrix of \mathbf{M} , i.e. $\mathbf{M}_{(2,1)}^M$. The efficiency can then be written in the form

$$\eta = 2\Gamma \frac{\text{Det}[\mathbf{M}_{(2,1)}^M]}{\text{Det}[\mathbf{M}]}. \quad (\text{E15})$$

We note that the integral only converges if the eigenvalues $\epsilon_M^{(j)}$ all have negative real parts, which is true for a system with dissipation and without driving.

Appendix F: Inverse Laplace Transform of $\langle a^\dagger a(s) \rangle$

The Laplace transform $\langle a^\dagger a(s) \rangle$ has form

$$\langle a^\dagger a(s) \rangle = \frac{Q(s)}{D(s)}, \quad (\text{F1})$$

where

$$Q(s) = \sum_{j=0}^{N-1} a_j s^j, \quad D(s) = \prod_{i=1}^N (\epsilon_M^{(i)} - s). \quad (\text{F2})$$

If we assume there are no degeneracies, $\epsilon_M^{(i)}$ ($i = 1, \dots, N$) are completely distinct and we can rewrite Eq. (F1) in the form

$$\langle a^\dagger a(s) \rangle = \sum_{j=1}^N \frac{C_j}{(\epsilon_M^{(j)} - s)}. \quad (\text{F3})$$

By multiplying both sides of Eq. (F3) by $(\epsilon_M^{(j)} - s)$ and substituting $s = \epsilon_M^{(j)}$, we find C_j as,

$$C_j = \left[(\epsilon_M^{(j)} - s) \frac{Q(s)}{D(s)} \right]_{s=\epsilon_M^{(j)}}, \quad (\text{F4})$$

and we can apply an inverse Laplace transform to Eq. (F3) to obtain

$$\langle a^\dagger a(t) \rangle = - \sum_{j=1}^N C_j e^{\epsilon_M^{(j)} t}, \quad (\text{F5})$$

We can integrate this to find the efficiency

$$\eta = 2\Gamma \sum_{j=1}^N \frac{C_j}{\epsilon_M^{(j)}}. \quad (\text{F6})$$

We can simplify this by equating equations Eq. (F1) and (F3) to find

$$\frac{\sum_{j=0}^{N-1} a_j s^j}{\prod_{i=1}^N (\epsilon_M^{(i)} - s)} = \sum_{j=1}^N \frac{C_j}{(\epsilon_M^{(i)} - s)}, \quad (\text{F7})$$

which holds for all s . So if we take $s = 0$ we obtain

$$\eta = 2\Gamma \sum_{j=1}^N \frac{C_j}{\epsilon_M^{(j)}} = 2\Gamma \frac{a_0}{\prod_{i=1}^N \epsilon_M^{(i)}}. \quad (\text{F8})$$

If there are degeneracies in $\epsilon_M^{(i)}$ ($i = 1, \dots, N$), for example r -fold degeneracy of $\epsilon_M^{(d)}$ ($d = N - r + 1$), Eq. (F3) becomes

$$\langle a^\dagger a(s) \rangle = \sum_{\substack{j=1 \\ j \neq d}}^{N-r} \frac{C_j}{(\epsilon_M^{(j)} - s)} + \sum_{i=1}^r \frac{k_i}{(\epsilon_M^{(d)} - s)^i}, \quad (\text{F9})$$

$$C_j = \left[(\epsilon_M^{(j)} - s) \frac{Q(s)}{D(s)} \right]_{s=\epsilon_M^{(j)}}, \quad (\text{F10})$$

$$k_i = \frac{1}{(r-i)!} \frac{d^{r-i}}{ds^{r-i}} \left[(\epsilon_M^{(d)} - s)^r \frac{Q(s)}{D(s)} \right]_{s=\epsilon_M^{(d)}}, \quad (\text{F11})$$

where the first term in Eq. (F9) gives the contribution from the non-degenerate eigenvalues, and the second gives the contribution from the degenerate eigenvalues. An inverse Laplace transformation on Eq. (F9) gives

$$\langle a^\dagger a(t) \rangle = - \sum_{\substack{j=1 \\ j \neq d}}^{N-r} C_j e^{\epsilon_M^{(j)} t} + \sum_{i=1}^r \frac{(-1)^i k_i t^{(i-1)}}{(i-1)!} e^{\epsilon_M^{(d)} t}, \quad (\text{F12})$$

which we integrate to obtain the efficiency as

$$\eta = 2\Gamma \left(\sum_{\substack{j=1 \\ j \neq d}}^{N-r} \frac{C_j}{\epsilon_M^{(i)}} + \sum_{i=1}^r \frac{k_i}{(\epsilon_M^{(d)})^i} \right). \quad (\text{F13})$$

In integrating Eq. (F12) we have used the following

$$\int_0^\infty \frac{t^n}{n!} e^{at} dt = \left(\frac{-1}{a} \right)^n, \quad (\text{F14})$$

for $n = 0, 1, 2, \dots$ and $\text{Re}[a] < 0$. Now we can use the same technique as before, by equating Eq. (F1) and Eq. (F9), for $s = 0$, we find

$$\eta = 2\Gamma \sum_{\substack{j=1 \\ j \neq d}}^{N-r} \frac{C_j}{\epsilon_M^{(i)}} + \sum_{i=1}^r \frac{k_i}{(\epsilon_M^{(d)})^i} = 2\Gamma \frac{a_0}{\prod_{i=1}^N \epsilon_M^{(i)}}, \quad (\text{F15})$$

where a_0 is defined in Eq. (E11). It should be noted that the result in Eq. (F15) with degeneracies is the same as the result in Eq. (F8) without degeneracies.

-
- [1] N. Lambert, Y.-N. Chen, Y.-C. Cheng, C.-M. Li, G.-Y. Chen, and F. Nori, Quantum biology, *Nature Physics* **9**, 10 (2013).
 - [2] J. Cao, R. J. Cogdell, D. F. Coker, H.-G. Duan, J. Hauer, U. Kleinekathöfer, T. L. Jansen, T. Mančal, R. D. Miller, J. P. Ogilvie, *et al.*, Quantum biology revisited, *Science Advances* **6**, eaaz4888 (2020).
 - [3] S. Lloyd, Quantum coherence in biological systems, *Journal of Physics: Conference Series* **302**, 12037 (2011).
 - [4] G. D. Scholes, G. R. Fleming, A. Olaya-Castro, and R. Van Grondelle, Lessons from nature about solar light harvesting, *Nature chemistry* **3**, 763 (2011).
 - [5] T. Mirkovic, E. E. Ostroumov, J. M. Anna, R. Van Grondelle, Govindjee, and G. D. Scholes, Light absorption and energy transfer in the antenna complexes of photosynthetic organisms, *Chemical reviews* **117**, 249 (2017).
 - [6] Y.-C. Cheng and G. R. Fleming, Dynamics of light harvesting in photosynthesis, *Annual review of physical chemistry* **60**, 241 (2009).
 - [7] H. Haken and G. Strobl, An exactly solvable model for coherent and incoherent exciton motion, *Zeitschrift für Physik A Hadrons and nuclei* **262**, 135 (1973).
 - [8] Z.-Z. Li, L. Ko, Z. Yang, M. Sarovar, and K. B. Whaley, Interplay of vibration- and environment-assisted energy transfer, *New Journal of Physics* **24**, 33032 (2022).
 - [9] L. Chen, P. Shenai, F. Zheng, A. Somoza, and Y. Zhao, Optimal energy transfer in light-harvesting systems, *Molecules* **20**, 15224 (2015).
 - [10] S.-J. Xiong, L. Chen, and Y. Zhao, Dephasing and dissipation in a source-drain model of light-harvesting systems, *ChemPhysChem* **15**, 2859 (2014).
 - [11] P. Rebentrost, M. Mohseni, I. Kassal, S. Lloyd, and A. Aspuru-Guzik, Environment-assisted quantum transport, *New Journal of Physics* **11**, 033003 (2009).
 - [12] M. B. Plenio and S. F. Huelga, Dephasing-assisted transport: quantum networks and biomolecules, *New Journal of Physics* **10**, 113019 (2008).
 - [13] A. W. Chin, A. Datta, F. Caruso, S. F. Huelga, and M. B. Plenio, Noise-assisted energy transfer in quantum networks and light-harvesting complexes, *New Journal of Physics* **12**, 65002 (2010).
 - [14] P. W. Anderson, Absence of diffusion in certain random lattices, *Physical review* **109**, 1492 (1958).
 - [15] L. Novo, M. Mohseni, and Y. Omar, Disorder-assisted quantum transport in suboptimal decoherence regimes, *Scientific Reports* **6**, 18142 (2016).
 - [16] M. Žnidarič and M. Horvat, Transport in a disordered tight-binding chain with dephasing, *The European Physical Journal B* **86**, 67 (2013).
 - [17] M. Mohseni, A. Shabani, S. Lloyd, Y. Omar, and H. Rabitz, Geometrical effects on energy transfer in disordered open quantum systems, *The Journal of chemical physics* **138** (2013).
 - [18] E. Zerah-Harush and Y. Dubi, Effects of disorder and interactions in environment assisted quantum transport, *Physical Review Research* **2**, 023294 (2020).
 - [19] C. Maier, T. Brydges, P. Jurcevic, N. Trautmann, C. Hempel, B. P. Lanyon, P. Hauke, R. Blatt, and C. F. Roos, Environment-assisted quantum transport in a 10-qubit network, *Physical review letters* **122**, 050501 (2019).
 - [20] S. Niwa, L.-J. Yu, K. Takeda, Y. Hirano, T. Kawakami, Z.-Y. Wang-Otomo, and K. Miki, Structure of the lh1-rc complex from thermochromatium tepidum at 3.0 Å, *Nature* **508**, 228 (2014).
 - [21] L.-J. Yu, M. Suga, Z.-Y. Wang-Otomo, and J.-R. Shen, Structure of photosynthetic lh1-rc supercomplex at 1.9 Å resolution, *Nature* **556**, 209 (2018).
 - [22] L.-N. Liu, L. Bracun, and M. Li, Structural diversity and modularity of photosynthetic rc- lh1 complexes, *Trends in Microbiology* **32**, 38 (2024).
 - [23] S. Yang, D. Xu, Z. Song, and C. Sun, Dimerization-assisted energy transport in light-harvesting complexes, *The Journal of chemical physics* **132** (2010).
 - [24] H. Dong, D. Z. Xu, J. F. Huang, and C. P. Sun, Coherent excitation transfer via the dark-state channel in a bionic system, *Light: Science and Applications* **1**, 10.1038/lsa.2012.2 (2012).
 - [25] J. Strümpfer, M. Šener, and K. Schulten, How quantum coherence assists photosynthetic light-harvesting, *Journal of Physical Chemistry Letters* **3**, 536 (2012).
 - [26] S. Alexander, R. Andrews, O. Fox, and S. Sarkar, Quantum excitation transfer in an artificial photosynthetic light-harvesting system, *Phys. Rev. A* **112**, 023711 (2025).
 - [27] Q. S. Tan and L. M. Kuang, Environment-assisted excitation energy transfer in lh1-rc-type and lh2-type trimers, *Science China: Physics, Mechanics and Astronomy* **55**, 1541 (2012).
 - [28] C. Chuang and P. Brumer, Lh1-rc light-harvesting photocycle under realistic light-matter conditions, *The Journal of Chemical Physics* **152**, 154101 (2020).
 - [29] E. Wyke, A. Aiyejina, and R. Andrews, Disorder-assisted energy transfer in the lh1-rc complex with a gaussian

- laser pulse, in *Frontiers in Optics* (Optica Publishing Group, 2022) pp. JW4B–12.
- [30] G. Trinkunas and A. Freiberg, A disordered polaron model for polarized fluorescence excitation spectra of lh1 and lh2 bacteriochlorophyll antenna aggregates, *Journal of luminescence* **119**, 105 (2006).
 - [31] R. van Grondelle and V. Novoderezhkin, Dynamics of excitation energy transfer in the lh1 and lh2 light-harvesting complexes of photosynthetic bacteria, *Biochemistry* **40**, 15057 (2001).
 - [32] H.-P. Breuer and F. Petruccione, *The Theory of Open Quantum Systems* (Oxford University Press, 2006).
 - [33] C. Gardiner and P. Zoller, *The Quantum World of Ultra-Cold Atoms and Light Book I: Foundations of Quantum Optics* (IMPERIAL COLLEGE PRESS, 2014).
 - [34] E. Wyke, A. Aiyejina, R. Andrews, and A. D. Greentree, Transfer efficiency in a pulsed light-harvesting trimer system, *J. Opt. Soc. Am. B* **41**, C158 (2024).
 - [35] T. Holstein and H. Primakoff, Field dependence of the intrinsic domain magnetization of a ferromagnet, *Phys. Rev.* **58**, 1098 (1940).